Fatigue Performance of Engineered Polymer Composite Railroad Ties Under Simulated Railroad Track Conditions

Jubair Ahmad Musazay[1,2,*]

[1] Department of Civil and Environmental Engineering, Pennsylvania State University, University Park, PA 16802, USA

[2] Rail Transportation Engineering, Pennsylvania State University, Altoona, PA 16601, USA

[*] Corresponding: jqm6784@psu.edu, ORCID: 0000-0002-7030-868X

Abstract

The fatigue performance of Engineered Polymer Composite (EPC) railroad ties under realistic track loading and support conditions remains an important consideration for their structural performance and durability. This study evaluated EPC railroad ties manufactured from recycled polymers and mineral fillers through initial mechanical characterization, small-scale fatigue testing, full-scale fatigue testing, post-fatigue mechanical characterization, and forensic investigations. Small-scale specimens were subjected to strain-controlled four-point bending fatigue tests at different strain amplitudes, with extended testing continued for over one million cycles. The full-scale experiment consisted of four EPC ties supporting two rails inside a ballast box, with two hydraulic actuators simulating railroad bogie loading for over 350,000 cycles per actuator. Track displacement, flexural and shear strains, and distributed fiber optic measurements were used to characterize the structural response, supplemented by analytical evaluation and temperature correlation analysis. Small-scale fatigue testing demonstrated relatively stable flexural stiffness, with apparent stiffness-based damage remaining below 1% and partial stiffness recovery observed during cyclic loading. The full-scale experiment revealed differential track settlement and nonuniform flexural and shear strain responses, while analytical and experimental results highlighted the importance of localized shear deformation near the rail seats. Strong correlations were also observed between outdoor air temperature and daily mean recorded strains, although potential gauge-related effects could not be independently quantified. Post-fatigue mechanical testing showed average reductions of 6.35% in modulus of elasticity and 33.14% in modulus of rupture relative to separate unfatigued specimens. Forensic examination further revealed substantial manufacturing defects in a tie that fractured during the early stages of testing. Overall, the findings demonstrate the importance of considering localized flexural and shear strain response, track support conditions, and manufacturing quality alongside conventional mechanical characterization when evaluating the fatigue performance of EPC railroad ties.

Keywords: EPC Railroad Ties, Fatigue Performance, Shear Stress, Flexural Stress

1.0 Introduction

Railroad ties are critical components of railway track infrastructure, responsible for maintaining track gauge and geometry, supporting the rails, and transferring train loads to the underlying ballast and subgrade. Wood has traditionally been the predominant tie material in North America due to its established historical performance. However, biological deterioration, environmental concerns associated with preservative treatments, and increasing axle load demands on railroad infrastructure have encouraged the development of alternative tie materials, including concrete, steel, and composites (*1–3*). Among these alternatives, Engineered Polymer Composite (EPC) railroad ties have attracted considerable interest in recent decades, partially due to their potential resistance to biological deterioration and moisture related damage, their resiliency and opportunity to incorporate recycled materials (*4*, *5*). Their compatibility with existing railroad infrastructure and potential integration with advanced structural health monitoring systems are additional advantages. Unlike conventional tie materials, EPC railroad ties encompass a broad range of material compositions, manufacturing processes, and structural configurations. Their constituents may include recycled or virgin polymers, mineral fillers, rubber particles, reinforcing fibers, and various additives. Depending on the formulation and intended application, composite ties may be prepared through additive manufacturing, extrusion molding, fiber-reinforced members, or layered and reinforced structural systems (*3*). These variations can significantly influence stiffness, strength, deformation characteristics, and failure mechanisms. Ju et al. (*6*), for example, demonstrated that the type, particle size, and proportion of mineral fillers influence the mechanical properties of recycled plastic composites, with increased filler content improving stiffness while potentially increasing brittleness. Other investigations have demonstrated the influence of fiber reinforcement, material combinations, and structural configurations on the mechanical performance of alternative railway sleepers (*7*, *8*). Consequently, EPC ties should not be treated as a mechanically uniform material category, and findings obtained from one formulation or structural configuration may not be directly transferable to another.

Despite their potential advantages, EPC railroad ties have demonstrated varying levels of success in laboratory investigations and field applications. Early evaluations at the Facility for Accelerated Service Testing (FAST) indicated that certain plastic-composite tie systems could provide vertical track stiffness comparable to conventional wood tie track (*9*). However, subsequent investigations identified cracking, fastening-related deterioration, permanent deformation, and other performance concerns associated with different EPC technologies (*3*, *10*, *11*). Particularly, center cracking and spike-hole cracking have been identified as important failure modes in North American installations. FRA-sponsored investigations reported that these failures developed under repeated traffic loading despite measured in-track bending stresses remaining below the ties' ultimate static strength, suggesting fatigue related deterioration (*12*, *13*). Internal voids and manufacturing irregularities have also been associated with cracking in some EPC tie systems. Furthermore, investigations of alternative composite sleepers have identified longitudinal shear cracking and other failure mechanisms that differ considerably among materials and structural configurations (*14–16*). These findings emphasize the importance of evaluating localized damage mechanisms and the limitations of relying exclusively on conventional mechanical properties to predict long-term structural performance.

The American Railway Engineering and Maintenance-of-Way Association (AREMA)(*17*) provides recommendations for evaluating EPC railroad ties through mechanical and functional tests, including center negative bending, rail seat bending, rail seat compression, and fastening related performance. Although these tests establish important material and structural properties, their relationship with long-term performance under repeated train loading remains incompletely understood. AREMA acknowledges that performance criteria have not been fully developed for EPC ties across all evaluative tests and that laboratory testing is not intended to reproduce the complete operating and loading environment (*17*). Furthermore, ultimate flexural strength determined through static bending tests may not adequately characterize damage mechanisms developing under lower but repeated stresses. Recognizing these limitations, previous researchers have investigated alternative loading arrangements and fatigue testing

procedures intended to reproduce more representative bending conditions and failure mechanisms (*11*, *12*, *18*) . Nevertheless, the interaction between tie deformation, ballast support, load distribution, and localized strain response remains an important consideration when relating laboratory qualification results to actual track performance.

Several studies have investigated the cyclic and fatigue performance of polymer composite railroad ties using different materials, loading configurations, and performance indicators. Lotfy and Issa (19) evaluated an HDPE tie and fastening assembly under three million loading cycles and reported satisfactory performance with limited deterioration. Salih et al. (*15*) proposed a five-point bending test to reproduce the positive rail seat and negative center bending moments experienced by railway sleepers, while subsequent investigations demonstrated differences in failure mechanisms among timber, plastic, and reinforced composite sleepers, including permanent deformation and longitudinal shear cracking. In a broader investigation, Salih (*14*, *16*) evaluated small-scale and full-scale fatigue behavior and identified differences in the rate of degradation between specimen sizes and composite sleeper technologies. More recently, Gao and McHenry (12) developed a four-point bending fatigue procedure addressing EPC tie center cracking and investigated modified cyclic testing for deterioration near the rail seat and fastening system. Collectively, these studies demonstrate the importance of selecting fatigue testing methods that reflect the material characteristics, loading configuration, and governing failure mechanisms of the tie system.

An additional challenge arises from the time- and temperature-dependent behavior of polymeric materials. Unlike predominantly elastic materials, polymers can exhibit viscoelastic deformation, creep, stress relaxation, and hysteretic energy dissipation under repeated loading. Amjadi and Fatemi (2020)(20) demonstrated that the fatigue behavior of HDPE is influenced by temperature, loading frequency, mean stress, and manufacturing technique. Van Belkom et al. (21) further showed that continuous cyclic loading of polymer railway sleepers can produce self-heating and accumulated deformation that may differ from their response under intermittent train traffic. The authors proposed intermittent loading to reduce these effects while maintaining loading rates representative of railway service. These findings indicate that polymer fatigue performance depends not only on applied load and the number of cycles but also on loading history, frequency, temperature, and time-dependent deformation. Accordingly, reductions in stiffness and changes in measured strain under repeated loading do not necessarily represent irreversible fatigue damage, emphasizing the importance of distinguishing cyclic response, recoverable deformation, and progressive structural deterioration.

Although previous studies have investigated EPC tie material properties, fatigue behavior, and field performance, additional experimental evidence is needed to connect material-level cyclic response with structural behavior under simulated track loading and support conditions. In particular, the evolution of flexural and shear strains and their changes with ambient temperature, the influence of nonuniform support and load distribution, and the residual mechanical performance of EPC ties following repeated loading warrant further investigation. The objective of this study is evaluating an EPC railroad tie formulation through initial mechanical characterization, small-scale strain-controlled fatigue testing, and full-scale cyclic loading within a ballast box track assembly. The investigation combines conventional strain measurements, distributed fiber optic sensing, analytical evaluation, and post-fatigue mechanical and forensic assessments to characterize both localized and overall structural responses. It aims to provide an integrated experimental assessment of fatigue related behavior and identify factors influencing the structural performance of the investigated EPC formulation.

2.0 Materials and Methodology

In this study, Engineered Polymer Composite (EPC) railroad ties manufactured from recycled materials were evaluated through a series of laboratory tests to characterize their initial mechanical properties, fatigue response, and post-fatigue mechanical performance.

2.1 EPC Railroad Tie Materials and Manufacturing

The EPC railroad ties evaluated in this study were manufactured from a blend of recycled materials consisting of more than 60% high-density polyethylene (HDPE), selected as the primary polymer matrix for EPC railroad ties (*17*), with polystyrene (PS) and talc as the remaining major constituents, each accounting for approximately 20% of the composition. The recycled plastics were irregularly shaped, shredded particles, whereas talc was added in powdered form as a mineral filler to increase the stiffness of the resulting composite. The formulation was selected from an experimental matrix of more than 40 candidate compositions based on its comparatively favorable performance during preliminary small-scale testing and was subsequently advanced to full-scale tie production and evaluation. To produce the specimens, the constituents were mixed in the hopper of a plastic extruder and extruded at approximately 450 °F (230 °C) into molds. The resulting ties measured approximately 9 × 7 × 108 in. (229 × 178 × 2743 mm). The experimental design for this study is summarized in Table 1.

Table 1: Research Experimental Design

Stage	Purpose	Main Output
Initial three-point bending test	Mechanical characterization and material strength	Initial stress-Strain behavior, Modulus of Elasticity (MOE), and Modulus of Rupture (MOR)
Rail seat (plate area) compression test	Characterization of tie's compressive response	Elastic deformation of tie under applied load
Small scale fatigue test	Material level characterization of cyclic response	Flexural stiffness retention and apparent stiffness-based damage
Ballast box fatigue test	Full-scale cyclic evaluation under simulated track loading and support conditions	Track settlement and changes in stiffness, localized flexural and shear response of EPC ties using strain gauges and distributed response using fiber optic sensor
Post-fatigue three-point bending test	Residual mechanical response following fatigue loading	Residual MOE, MOR and changes relative to the initial condition

2.2 Mechanical Characterization

The EPC ties were initially evaluated for flexural strength using the center negative three-point bending test specified in Chapter 30 of the AREMA Manual (*17*). The test configuration and fixture dimensions are shown in Figure 1. Each tie was loaded to rupture using a 220-kip (979-kN) hydraulic actuator at a deflection rate of 5 in/min (127 mm/min). The load displacement data recorded by the actuator was used to determine the flexural response of the tie, with the downward displacement representing the midspan deflection relative to the supports. The same test procedure was subsequently used for post-fatigue mechanical characterization.



Figure 1: Three-point bending test for one of the EPC railroad ties

Mechanical properties were determined from the recorded load-displacement response using the procedures recommended by AREMA (*17*). The modulus of elasticity (MOE) was calculated as

$$MOE = \frac{mL^3}{48I}$$

where m is the slope of the load–deflection curve between the load levels corresponding to flexural stresses of 200 psi (1.38 MPa) and 600 psi (4.15 MPa), L is the support span, and I is the moment of inertia of the tie cross section. ASTM D6109 provides a toe-region correction for polymeric specimens; however, this correction was not applied because the measured load–deflection response did not exhibit a conventional toe region consistent with the standard definition. The modulus of rupture (MOR) was calculated as

$$MOR = \frac{3PL}{2bd^2}$$

where P is the maximum applied load, b is the tie width, and d is the tie depth. Although other approaches may be used to characterize the stiffness and strength of polymer composites, the AREMA procedures were adopted to maintain consistency with current railroad tie evaluation practices.

As part of the initial mechanical characterization, rail seat (plate area) compression testing was also conducted in accordance with AREMA procedures. The full-scale tie was loaded using a 220-kip (979-kN) hydraulic actuator through a 1-in. (25.4-mm) thick unspiked steel loading plate measuring 14 × 7.75 in. (356 × 197 mm). The load increased to 100-kip (445 kN) in 20-kip (89-kN) increments, with approximately 45 s between successive load increments. Actuator displacement was recorded throughout the test to characterize the local compressive response of the tie beneath the loading plate.

Additionally, bulk density and specific gravity of the same EPC formulation was determined using smaller size samples, measuring about 3.5 × 3.5 × 16 in. (89 × 89 × 406 mm). These were determined using the displacement principles defined in ASTM D6111. Because the specimens had a specific gravity below unity,

supplemental steel weights (sinkers) were secured to the specimens to maintain complete submersion during testing. The sinkers and associated securing tape were weighed separately, and their contribution was accounted for in the submerged weight measurements.

2.3 Small-Scale Fatigue Testing

Small-scale fatigue testing was conducted to evaluate the cyclic response of the EPC material using four-point beam fatigue testing equipment primarily designed for viscoelastic materials such as asphalt mixtures. Specimens measuring 2.0 × 2.5 × 15.0 in. (50 × 63 × 380 mm) were cut from the full-scale ties, with the specimen dimensions selected to accommodate the geometric limitations of the testing apparatus (Figure 2). Tests were conducted in four-point bending under constant strain loading at 20 °C (68 °F) and a loading frequency of 10 Hz. Initial screening tests were performed at strain amplitudes of 100, 300, 500, and 800 με for approximately 5,000 cycles at each level. Subsequently, longer duration fatigue tests were conducted at strain amplitudes of 800 and 1,000 με, with testing continued beyond one million loading cycles.

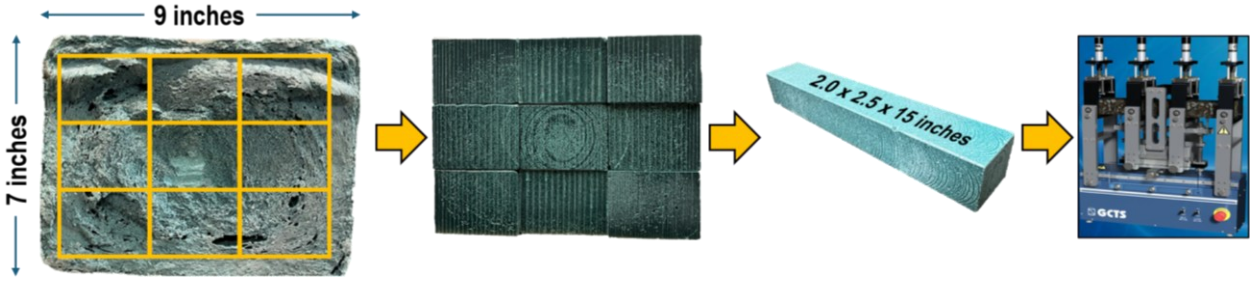


Figure 2: Small-scale fatigue test specimens and testing equipment

2.4 Full-Scale Fatigue Testing

A ballast box test setup was used to evaluate the cyclic response of the EPC railroad ties under loading and support conditions representative of the track environment. Unlike isolated beam testing, the ballast box configuration allowed the ties to interact with the ballast, rails, and fastening system during cyclic loading. The heavy-duty steel box measured approximately 13 ft (3.96 m) long, 11 ft (3.35 m) wide, and 4 ft (1.22 m) deep. The track consisted of four full-scale EPC ties supporting two rails fastened using conventional cut spikes and 14-in (0.36 m) tie plates. The ties were supported on approximately 14 in (0.36 m) of AREMA No. 3 ballast over a 12-in. (0.30 m) layer of compacted limestone sand, with the entire system resting on a concrete floor. The complete ballast box configuration and instrumented ties are shown in Figure 3.

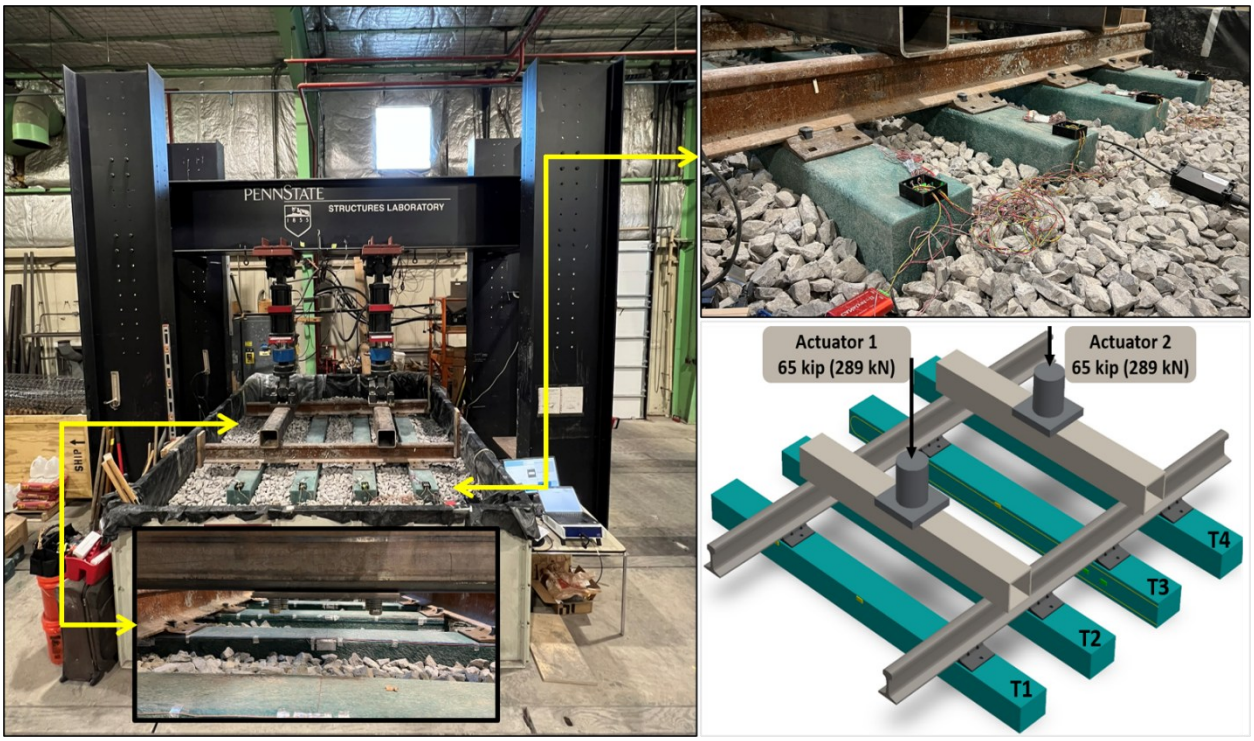


Figure 3: Ballast box testing setup with its simplified schematic

Cyclic loading was applied using two 110-kip (489 kN) MTS hydraulic actuators positioned above the rails. Each actuator transferred load through a steel spreader beam (Hollow Structural Section, HSS) to two rail contact locations, resulting in four loading points representing a two-axle railroad bogie loading configuration.

In railroad practice, when new ballast is laid, it is necessary to tamp, regulate, and stabilize the track before the trains are allowed to run. To simulate this in the ballast box before the fatigue test, an initial load was applied, which is referred to as the seating load in this study. This was conducted to promote immediate track settlement and establish a more consistent ballast support condition. The sequence consisted of 5,000 cycles at 35 kip (156 kN) per actuator and 2 Hz, followed by 5,000 cycles at 4 Hz and an additional 5,000 cycles at 2 Hz, with all loading applied sinusoidally. Main fatigue loading was subsequently applied at 65 kip (289 kN) per actuator and 2 Hz. The number of cycles applied during each test session varied, resulting in a total of 379,615 cycles per actuator over 10 testing sessions between August 13 and September 9, 2024. The loading details and test observations are summarized in Table 2. (S=seating load, F=main fatigue loading). The full-scale fatigue tests were conducted in an unconditioned high-bay laboratory with sufficient ventilation. The temperatures reported in Table 2 represent historical daily average outdoor air temperatures for State College, Pennsylvania, and are provided as an approximate indication of the ambient conditions during testing.

Table 2: Fatigue loading schedule

Test No.	Test Date	Load (kips) (2 Hz)	Cycles (Per Actuator)	Cumulative Cycles (Per Actuator)	T (°F [°C])	Track Observation
S-I	8/13/2024	35	5000	5000	66 (19)	Differential settlement observed between the actuators.
S-II	8/13/2024	35 (4 Hz)	5000	10000	66 (19)	Increased loading frequency was tested.

S-III	8/14/2024	35	5000	15000	68 (20)	Test continued after re-leveling, resulting in identical settlement
F-1	8/15/2024	65	50000	65000	70 (21)	The tie with the defect likely fractured. MTS data corrupted for this session. Other sensor data intact.
F-2	8/16/2024	65	50000	115000	70 (21)	Differential settlement continued. Test ran smoothly.
F-3	8/23/2024	65	50000	165000	62 (16)	Differential settlement continued. Test ran smoothly.
F-4	8/26/2024	65	50000	215000	74 (23)	Differential settlement continued. Test ran smoothly.
F-5	8/28/2024	65	75000	290000	76 (24)	Differential settlement continued. Test ran smoothly.
F-6	9/04/2024	65	50000	340000	59 (15)	Differential settlement continued. Test ran smoothly.
F-7	9/09/2024	65	39615	379615	57 (14)	Load spreader beam for Actuator 1 fractured, and the test was discontinued

2.4.1 Tie Instrumentation and Data Acquisition

The instrumentation plan for the fatigue test is shown in Figure 4. Each of the four EPC ties (labeled as T1 (exterior), T2 (interior), T3 (interior) and T4 (exterior)) were instrumented with three flexural strain gauges to monitor flexural response at critical locations along the tie. Two gauges, designated h1 and h3, were installed on the upper side surface at the two rail seat regions, while the h2 gauge was installed at the midpoint of the tie. Accordingly, the gauges are identified by tie number and location (e.g., T1h1, T1h2, and T1h3).

Tie 3 (T3) received additional instrumentation to provide more detailed characterization of the response near the rail seat region. Three shear strain gauges (labeled as SH1, SH2 and SH3) were installed at the neutral axis below the tie plate. As illustrated in Figure 4, SH1 was installed at the gauge side, SH2 beneath the midpoint, and SH3 at the field side of the tie plate. This arrangement was selected to characterize the variation in shear response across the rail seat region.

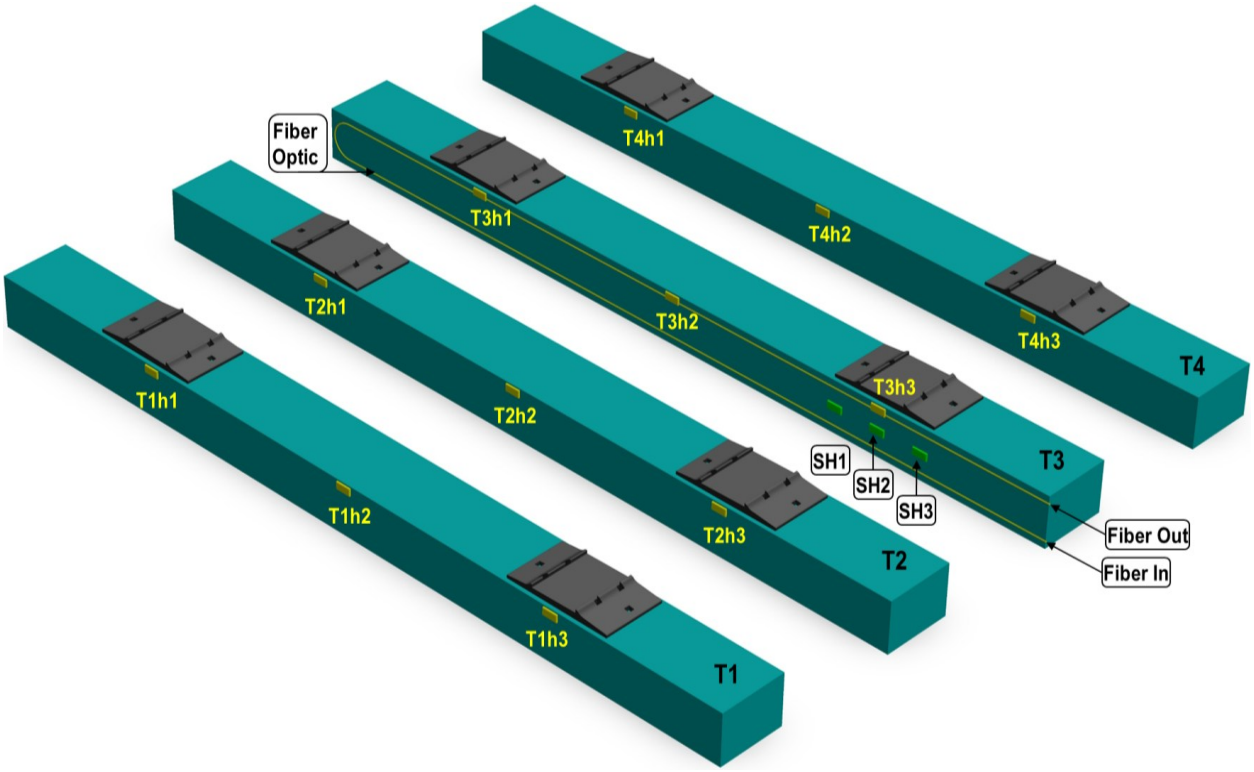


Figure 4: EPC ties instrumentation plan

T3 was also instrumented with a distributed fiber optic strain sensor to obtain a continuous longitudinal strain profile along the tie. The sensing fiber started at one end of the tie and extended longitudinally along the bottom of the side surface (approximately 0.5 inches (13 mm) offset from bottom) toward the opposite end, where it curved around the end of the tie and continued back along the top of the side surface (similar offset from the top side) toward the starting end. The fiber was attached using epoxy glue. This configuration provided distributed strain measurements for both the tension and compression sides of the tie. Fiber optic measurements were acquired using a LUNA ODiSI 6001 distributed sensing system at 20 Hz, with an active sensing length of approximately 5.3 m (17.4 ft) and a spatial measurement interval of approximately 5.2 mm (0.2 inches).

This instrumentation plan provided measurements at complementary structural scales. Load–displacement data recorded by the hydraulic actuators characterized the overall vertical response of the track system, the discrete longitudinal gauges measured localized flexural response at critical tie locations, the shear gauges characterized the rail seat shear response, and the distributed fiber optic sensor provided continuous spatial measurements of longitudinal strain along T3.

2.4.2 Analytical Evaluation of Flexural and Shear Response of a Railroad Tie

A representative EPC tie was evaluated analytically to estimate its flexural and shear response under simulated railroad loading conditions. Three loading configurations were considered as illustrated in Figure 5. The analysis used Euler–Bernoulli beam theory and classical beam equations to estimate flexural and shear strains for comparison with the experimental strain gauge measurements.

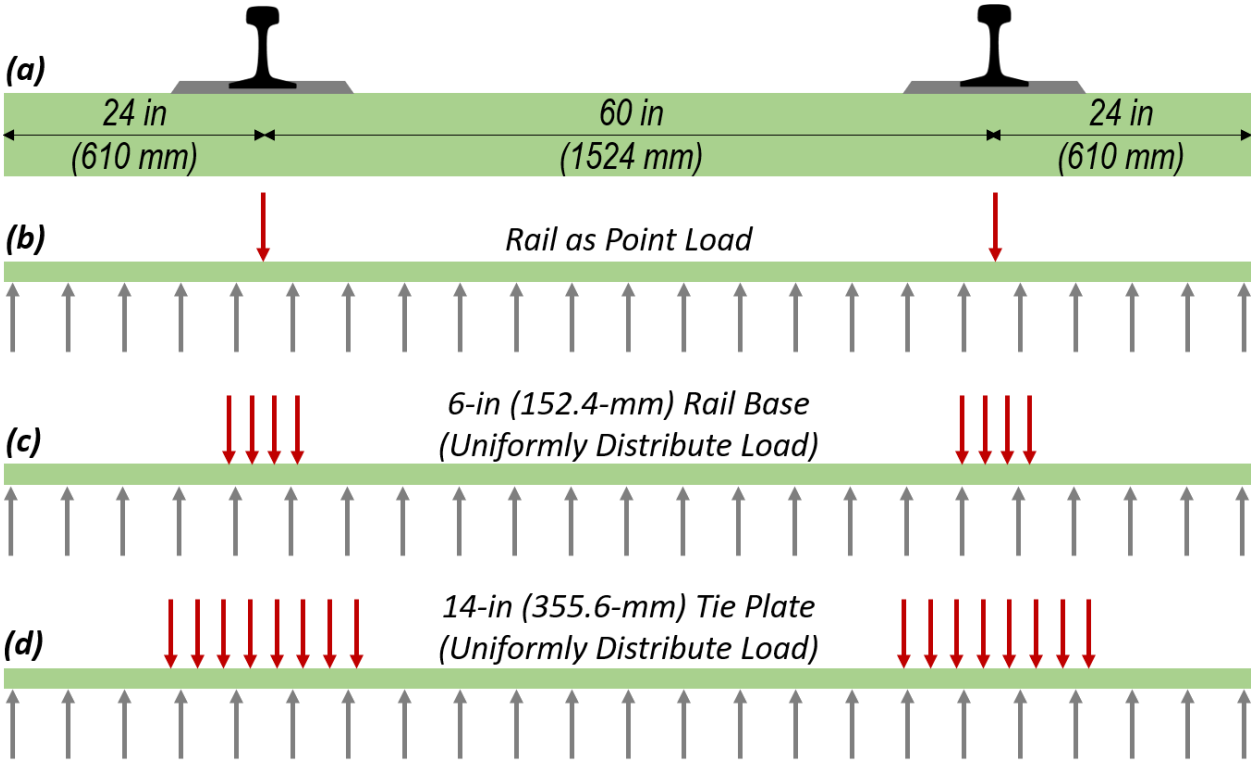


Figure 5. Geometry and loading configurations considered in the analytical evaluation: (a) EPC tie geometry and rail seat locations, (b) rail as concentrated load, (c) rail base as a uniformly distributed load, and (d) tie plate as uniformly distributed load

The analytical models were evaluated using a nominal load of 16.25 kip (72.3 kN) applied at each rail seat location, representing the load transferred through the rails to the tie. The applied loads were represented as concentrated loads, load uniformly distributed by rail base and tie plate widths. The ballast pressure was idealized as a uniformly distributed upward reaction along the entire tie length. The tie material was assumed to be homogeneous, isotropic, and linearly elastic. The modulus of elasticity was determined from the flexural testing described in Section 2.2, and an assumed Poisson's ratio of 0.45 was used to estimate the shear modulus.

For the concentrated load model illustrated in Figure 5(b), the shear force and bending moment distributions along the tie were determined using the following equations:

$$V(x) = \begin{cases} wx & 0 \le x < a \\ wx - P & a \le x < b \\ wx - 2P & b \le x \le L \end{cases}$$

$$M(x) = \begin{cases} \dfrac{wx^2}{2} & 0 \le x < a \\ \dfrac{wx^2}{2} - P(x-a) & a \le x < b \\ \dfrac{wx^2}{2} - P(x-a) - P(x-b) & b \le x \le L \end{cases}$$

Where, V(x) is the shear force at position x, M(x) is the bending moment at position x, x is the distance measured from the left end of the tie, w is the uniformly distributed upward ballast reaction, equal to 2P/L, P is the concentrated load applied at each rail seat, a is the location of the first rail seat, equal to (L − S)/2, b is the location of the second rail seat, equal to (L + S)/2, L is the total length of the tie, and S is the center-to-center spacing between the rail seats.

For the distributed loading models illustrated in Figures 5(c) and 5(d), the rail seat loads were assumed to be uniformly distributed over the 6-in. rail base and 14-in. tie plate widths, respectively. The shear force and bending moment distributions were determined using the following generalized equations:

$$V(x) = wx - q[\langle x - x_1\rangle - \langle x - x_2\rangle + \langle x - x_3\rangle - \langle x - x_4\rangle]$$

$$M(x) = \frac{wx^2}{2} - \frac{q}{2}[\langle x - x_1\rangle^2 - \langle x - x_2\rangle^2 + \langle x - x_3\rangle^2 - \langle x - x_4\rangle^2]$$

Where q is the uniformly distributed load intensity, calculated by dividing the load P by the contact width d, taken as 6 in. for the rail base and 14 in. for the tie plate. The variables x1 and x2 represent the beginning and end locations of the first distributed load, respectively, calculated by subtracting and adding half the contact width to the first rail seat location (a). Similarly, x3 and x4 represent the beginning and end locations of the second distributed load, calculated relative to the second rail seat location (b). The angle brackets denote Macaulay brackets, in which negative arguments are taken as zero while positive arguments retain their values. All other variables retain their previously defined meanings.

Subsequently, for each loading configuration, the calculated bending moments and shear forces were used to determine the extreme-fiber flexural stresses and maximum transverse shear stresses as follows.

$$\sigma(x) = \frac{M(x)c}{I}$$

$$\tau(x) = \frac{3V(x)}{2Bh}$$

$$\varepsilon(x) = \frac{\sigma(x)}{E}$$

$$\gamma(x) = \frac{\tau(x)}{G}$$

$$G = \frac{E}{2(1+\nu)}$$

Where σ(x) and τ(x) are the extreme-fiber flexural stress and maximum transverse shear stress, respectively; c is the distance from the neutral axis to the extreme fiber, equal to half the tie depth; I is the second moment of area of the rectangular cross section; B and h are the tie width and depth, respectively; ε(x) and γ(x) are the corresponding flexural and shear strains; E is the modulus of elasticity; G is the shear modulus; and ν is Poisson's ratio.

2.4.3 Correlation of Recorded Strain with Temperature

To investigate the relationship between temperature variations and recorded strain response, a correlation analysis was conducted using the daily mean outdoor air temperatures presented in Table 2. The temperature values were compared with the daily mean flexural strains at the rail seat (h1 and h3) and tie midspan (h2) locations, as well as the daily mean shear strain magnitudes from the three gauges (SH1, SH2, and SH3). Pearson correlation coefficients and linear regression were used to evaluate the relationships between temperature and recorded strain.

3.0 Results and Discussion

The experimental results are presented and discussed in the sequence of the testing program, beginning with the initial mechanical characterization of the EPC ties, followed by the small-scale fatigue testing, full-scale ballast box fatigue testing, and post-fatigue mechanical evaluation.

3.1 Initial Mechanical Performance

From the batch of six manufactured EPC railroad ties, two ties were randomly selected for initial flexural characterization using the procedure described in Section 2.2. Both ties were loaded to failure. A sample stress-strain response is presented in Figure 6. The resulting average modulus of elasticity (MOE) and modulus of rupture (MOR), together with their standard deviations, are summarized in Table 3. MOR exceeded the minimum design requirements, while MOE was above the higher value of the recommended range for EPC railroad ties specified in Chapter 30 of the AREMA Manual (Table 30-5-1) (*17*).

As shown in Figure 6, the stress-strain response of the EPC ties differed somewhat from the idealized response for polymeric materials illustrated in ASTM D6109, particularly in the toe region. The tested ties exhibited only a minor initial toe response. Such behavior is generally associated with test and specimen-related effects, including seating, alignment, slack, and internal voids, rather than intrinsic material response. AREMA therefore references the ASTM D6109 procedure for correcting the initial portion of the curve when an appreciable toe region is present. In the present analysis, however, no toe correction was applied because the observed toe regions were relatively minor, and the mechanical properties were calculated directly from the measured response. Application of the correction would produce a slightly steeper evaluated slope and, consequently, a higher MOE; therefore, the MOE values reported in Table 3 represent a conservative estimate of the tie stiffness.

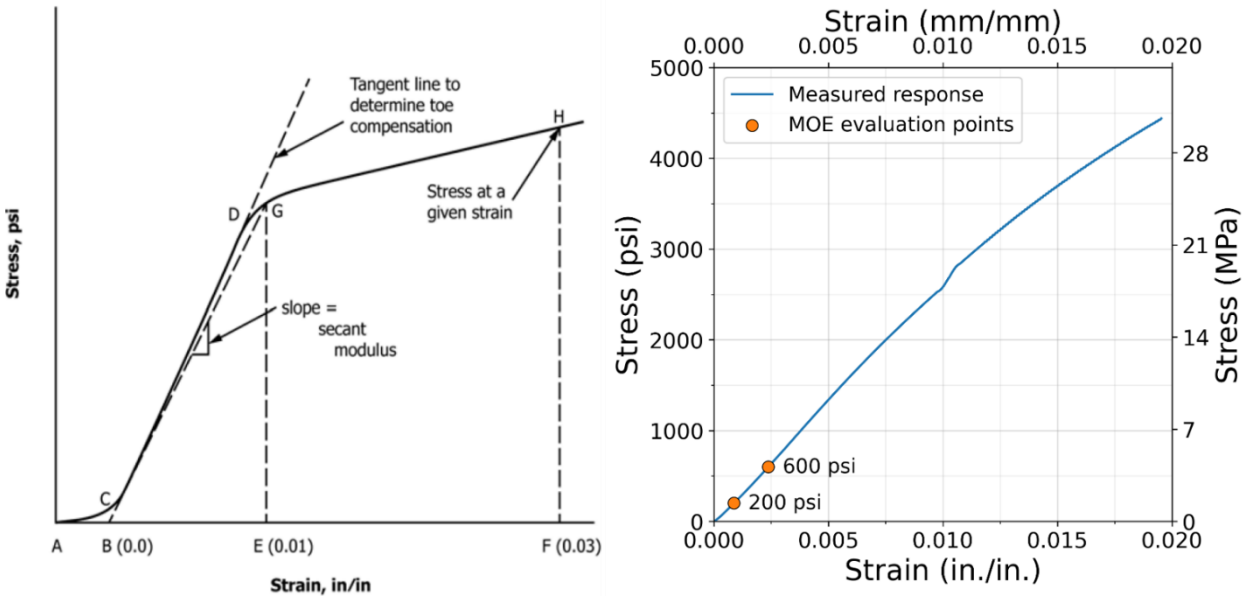


Figure 6: Idealized stress–strain response of polymeric composites and toe-region correction based on ASTM D6109 (left), and measured response of the EPC railroad ties evaluated in this study (right).

Furthermore, the measured load-displacement response from the rail seat compression test is presented in Figure 7, with the corresponding data reported in Table 3. Vertical displacement increased progressively with applied load, reaching a mean value of 0.2331 in. (5.92 mm) at the maximum applied load of 100 kip (445 kN) for three tests. This value remained below the AREMA maximum elastic deformation criterion of 0.25 in. (6.35 mm), indicating that the tie satisfied the rail seat compression requirement under the applied loading condition. The response exhibited no abrupt increase in deformation or other indication of unstable behavior up to the maximum load. This result also provided confidence that the subsequent ballast box fatigue loading would not introduce significant local compression damage at the rail seat. During the ballast box test, the 65-kip (289-kN) actuator load was distributed through the spreader beam to two rail loading points, resulting in approximately 32.5 kip (145 kN) at each rail. In conventional railroad track analysis, approximately 30% of an applied wheel load may be distributed to the tie directly beneath the wheel, corresponding to approximately 9.8 kip (44 kN) for the present loading configuration. However,

considering the relatively short rail section supported by only four ties, an equal distribution of the wheel load between the two adjacent ties was also considered. Under this assumption, each tie would carry approximately 16.25-kip (72 kN), still substantially below the 100-kip (445-kN) load applied during the rail seat compression test. Accordingly, local compressive deformation of the EPC ties beneath the rail seats during the ballast box fatigue test was expected to remain comparatively small and predominantly elastic.

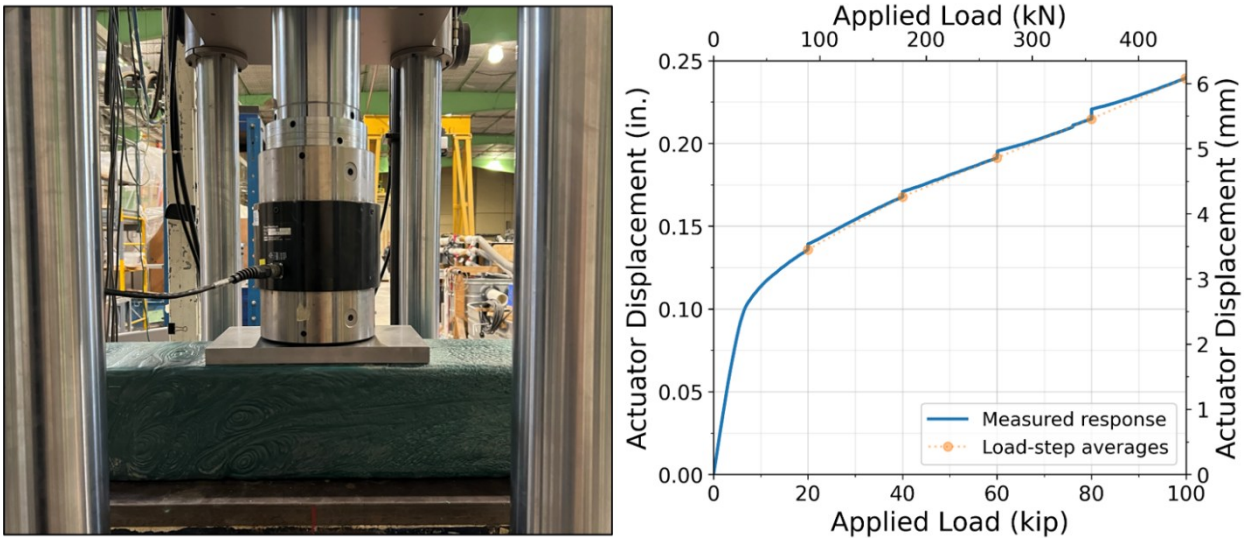


Figure 7: Rail seat compression test setup (left), and its load-displacement response (right)

Table 3: Initial mechanical strength of the developed tie

Engineering Properties	Mean Values	±SD	AREMA Range
Modulus of Elasticity, MOE	266,353 (1,836 MPa)	6,557 (45.2 MPa)	150,000 – 250,000 (1,034 MPa – 1,723 MPa)
Modulus of Rupture, MOR	3,491 (24 MPa)	946 (6.52 MPa)	≥ 2,500 (≥ 17.2 MPa)
Rail seat (plate area) compression	0.2331 in (5.92 mm)	0.0053 in (0.1346 mm)	< 0.25 in (6.35 mm)
Density (lb/ft^3)	61.95 (992.34 kg/m^3)	2.51 (40.21 kg/m^3)	N/A (ASTM D6111)
Specific Gravity	0.99	0.04	N/A (ASTM D6111)

3.2 Small-Scale Fatigue Response

Initially, fatigue screening was conducted at strain amplitudes of 100, 300, 500, and 800 με for 5,000 loading cycles. Figure 8 presents the corresponding flexural stiffness response in both absolute and normalized forms. Across all four strain levels, stiffness remained generally stable throughout the screening period, with only minor variations and no evidence of progressive degradation. The normalized stiffness remained close to its cycle-50 value for each specimen. The y-axis in Figure 8(b) was intentionally expanded to emphasize these small variations; however, the overall changes remained confined to a narrow range. Changes in stiffness were quantified using an apparent stiffness loss index, $D = 1 - S_N/S_{50}$, where S_{50} is the flexural stiffness at cycle 50, consistent with the normalization convention in AASHTO T 321, and S_N is the stiffness near the end of the screening test. The 500 and 800 με specimens exhibited stiffness reductions of approximately 0.25% and 0.41%, respectively, after 5,000 cycles. In contrast, the 100 and 300 με specimens showed essentially no stiffness loss, with the measured stiffness remaining at or slightly above the cycle-50 reference value.

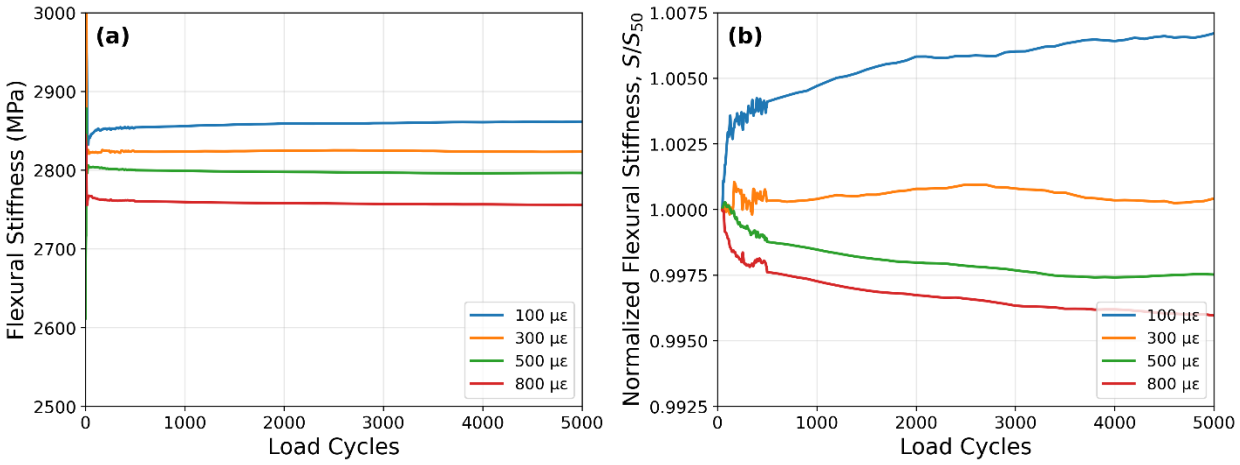


Figure 8: (a) Flexural stiffness and, (b) normalized flexural stiffness for the initial 5000 cycles

Subsequently, longer-duration fatigue tests were conducted at 800 and 1000 με for one million cycles. Figures 9-11 summarize the fatigue response in terms of deformation, flexural stiffness, and apparent stiffness-based damage, respectively. The y-axis in these figures is intentionally expanded to visualize the difference in the narrow band. As shown in Figure 9, both absolute and normalized deformation responses remained stable throughout the test duration.

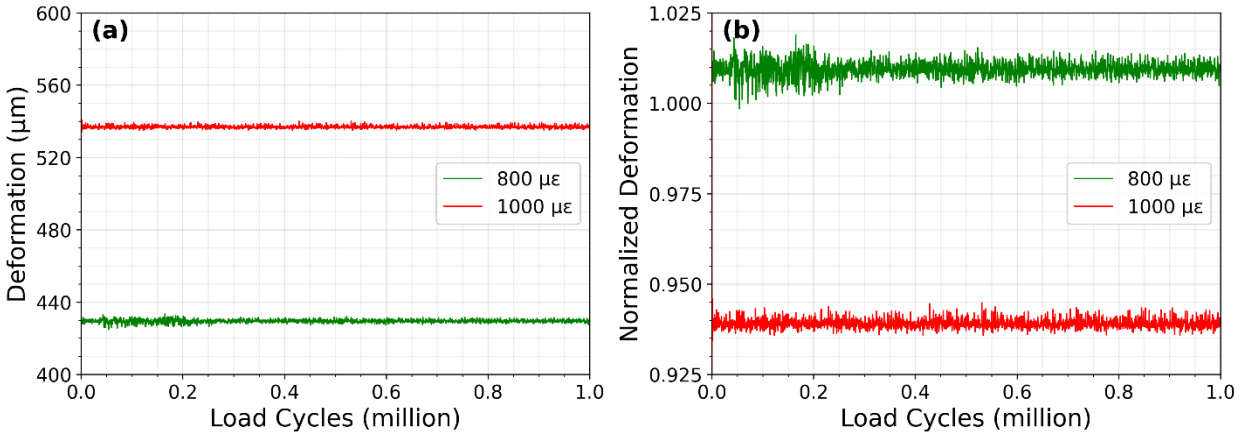


Figure 9: (a) Absolute deformation, and (b) normalized absolute deformation

The flexural stiffness response shown in Figure 10 remained relatively stable over one million loading cycles, with both specimens maintaining stiffness values within approximately 2700–2800 MPa. Both specimens exhibited an initial reduction in stiffness during the early stage of cyclic loading, followed by partial recovery and subsequent stabilization as testing progressed. The recovery seems more pronounced for the 800 με specimens, although neither specimen exhibited continued monotonic stiffness degradation over the investigated loading duration.

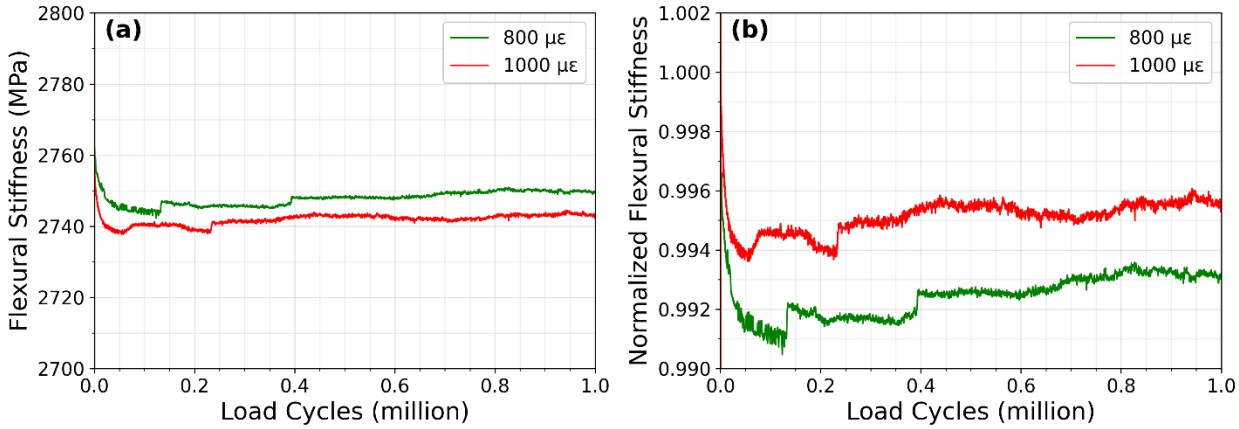


Figure 10: (a) Flexural stiffness, and (b) normalized flexural stiffness

Furthermore, apparent stiffness-based damage was calculated using the stiffness at cycle 50 as the reference value as $D(\%) = (1 - S_N/S_{50}) \times 100$. As shown in Figure 11, the apparent stiffness-based damage increased rapidly during the early portion of the test, reaching maximum values of approximately 0.95% for the 800 με specimen and 0.64% for the 1000 με specimen. These maxima occurred relatively early, at approximately 123,500 cycles and 54,500 cycles, respectively. Thereafter, the calculated damage decreased rather than progressively accumulating. By one million cycles, it had decreased to approximately 0.70% and 0.46% for the 800 and 1000 με specimens, respectively. This reduction indicates that at least part of the early stiffness loss was reversible, which is consistent with time-dependent recovery also observed during the full-scale ballast box fatigue test. Additionally, the larger apparent stiffness-based damage at the 800 με level does not indicate that the lower strain amplitude produced greater absolute material damage. The damage index represents the relative reduction in stiffness from each specimen's individual cycle 50.

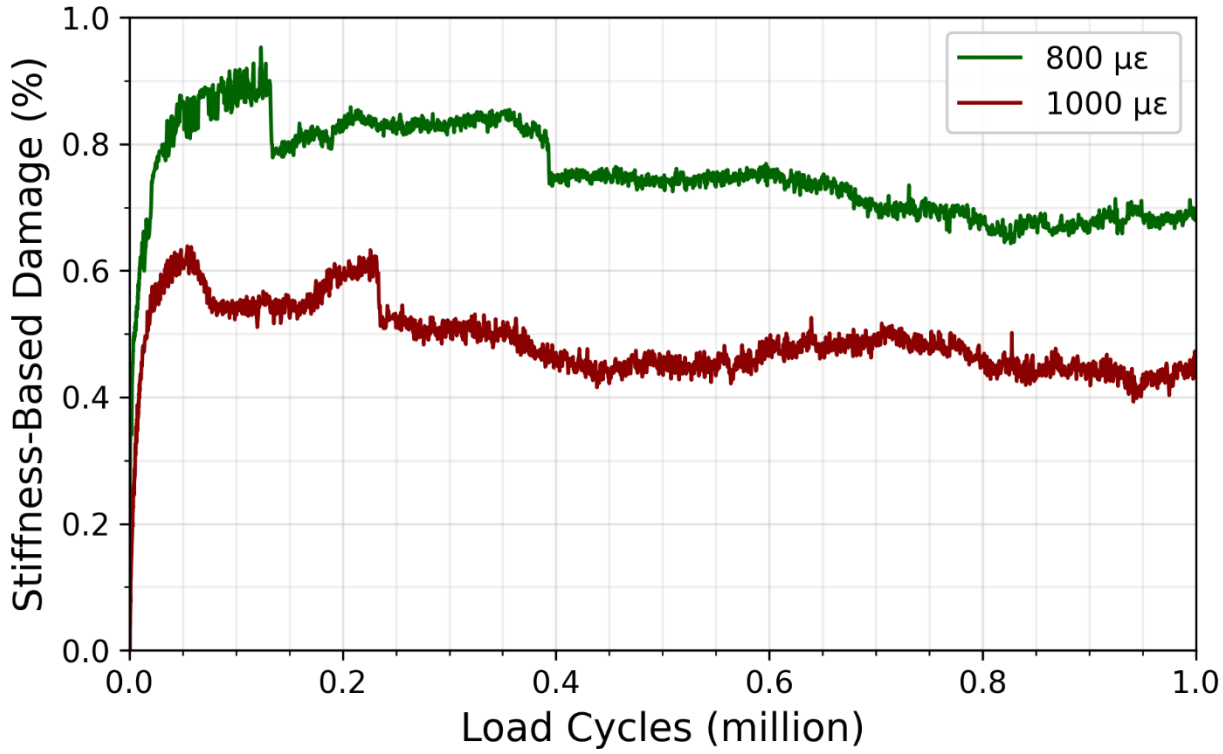


Figure 11: Apparent stiffness-based damage based on 800 and 1000 με strain levels

Overall, the small-scale fatigue tests demonstrated relatively stable flexural stiffness under the investigated strain amplitudes and loading duration, with no evidence of sustained progressive stiffness degradation. The fatigue response of the EPC ties under simulated railroad track conditions is evaluated in the following section using the full-scale ballast box experiment.

3.3 Full-Scale Fatigue Response

The fatigue performance of the EPC railroad ties was evaluated using data obtained from the flexural strain gauges, shear strain gauges, and fiber optic sensor during the full-scale ballast box test. The behavior of the supporting track system was examined to establish how the ballast and overall track stiffness evolved during repeated loading. Accordingly, the full-scale fatigue test results are presented first in terms of track settlement and equivalent track stiffness, followed by the measured flexural strain, shear strain, and fiber-optic strain response of the EPC ties.

3.3.1 Track Settlement and Stiffness

The first stage of the ballast box fatigue test analysis focused on the load-displacement data recorded by the MTS hydraulic actuators. These measurements were used to evaluate track settlement and changes in equivalent track stiffness throughout the fatigue test. Monitoring these parameters was important because the support conditions of the track, particularly ballast settlement and stiffness, directly influence the distribution of loads and the resulting response of the EPC ties.

The full-scale fatigue test was designed to simulate repeated railroad axle loading through the application of relatively high cyclic loads at a frequency representative of repeated loading associated with a moving train. Nominal actuator loads of 35 and 65 kip (156 and 289 kN) were selected for the seating and main fatigue loading stages, respectively. However, the actual peak loads achieved during cyclic loading depended on the loading frequency, as summarized in Table 4. At higher frequencies, the hydraulic actuators had less time within each loading cycle to develop the prescribed load before the loading direction was reversed, resulting in measured peak loads below the nominal values. Accordingly, a loading frequency of 2 Hz was selected for the main fatigue test to provide repeated loading at the intended rate while maintaining a substantial cyclic load magnitude.

Table 4: Effect of Loading Frequency on Achieved Cyclic Load in the MTS System

Applied Load (kip) (kN)	Loading Frequency (Hz)	Cycle Valley (kip) (kN)	Cycle Peak (kip) (kN)	Peak-to-Peak (kip)	Achieved Peak Load (%)
65 (289)	1.0	8.3 (37)	61.0 (271)	52.8 (235)	93.9%
60 (267)	1.5	2.3 (10)	47.8 (213)	45.5 (202)	79.6%
65 (289)	2.0	13.9 (62)	49.6 (221)	35.7 (159)	76.3%
35 (156)	2.0	8.2 (36)	28.1 (125)	19.9 (89)	80.4%
35 (156)	4.0	11.7 (52)	23.8 (106)	12.0 (53)	67.9%

Ballast settlement in this test was monitored using actuator's vertical displacement data, (δ_{MTS}). However, the vertical displacement includes the combined contributions of elastic deformation of the load spreader beam ($\delta_{spreader\ beam}$), EPC tie deformation (δ_{tie}), rail deflection (δ_{rail}), and ballast settlement, $\delta_{(ballast)}$. These components were estimated separately so that the settlement associated with ballast could be approximated as:

$$\delta_{ballast} = \delta_{MTS} - \left[\delta_{spreader\ beam} + \delta_{tie} + \delta_{rail}\right]$$

Subsequently, the elastic deformation of the load spreader beam was calculated using Euler–Bernoulli beam theory. The 8 × 8 × ½ in HSS (203 mm x 203 mm x 13 mm) spreader was idealized as a simply supported beam with a 60 in (1.524 m) span subjected to the 65-kip (289-kN) actuator nominal load at midspan, as

illustrated in Figure 12. Using deflection equation for a simply supported beam with point load, $\delta_{spreader\ beam} = (PL^3)/(48EI)$, the resulting elastic deflection was estimated to be 0.071 in (1.8034 mm).

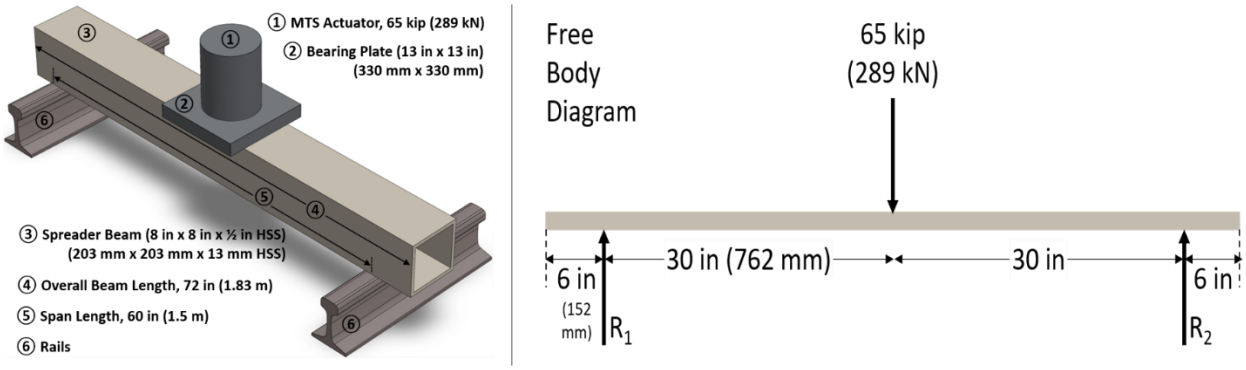


Figure 12: A model of one of the load spreader beams with its idealized FBD

Furthermore, the elastic deformation of the EPC ties was estimated using the load displacement response obtained from the rail seat compression test shown in Figure 7. Given a short rail section, the idealized nominal wheel load (32.5 kip, 145 kN) is assumed to be equally distributed to the two nearby ties, with each subjected to 16.25 kip (72 kN). Using the rail seat compression data and linearly interpolating between the corresponding data points, deformation of the EPC ties is approximately, $\delta_{tie} \approx 0.125\ in$ (3.175 mm).

On the other hand, although rail deflection in conventional track structures is commonly evaluated using beam on elastic foundation theory, the relatively short rail section and four discrete tie supports in the present experimental setup were represented using a finite Euler–Bernoulli beam model (Figure 13). Therefore, δ_{rail} is approximated to be 0.004 in (0.1016 mm).

Consequently, the ballast settlement is approximated as $\delta_{ballast} = \delta_{MTS} - 0.200$ for the 65-kip loading and $\delta_{ballast} = \delta_{MTS} - 0.108$ for the seating load (35 kip).

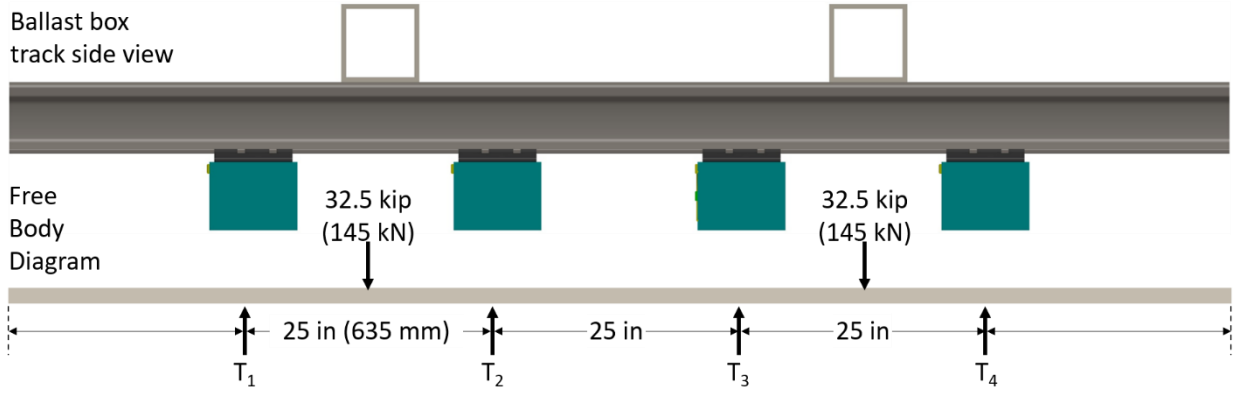


Figure 13: Side view of the track with ties, rail and spreader beams

Figure 14 shows the total vertical displacement and ballast settlement for the seating load. As shown in this figure the first 5,000 cycles at 35 kip (156 kN) and 2 Hz (Figure 14a) produced noticeable differential displacement between the two actuator locations. Due to symmetry in the track and loading, the actuators vertical displacement was expected to be similar, or almost identical. Differential displacement between the two actuator locations was also observed when the loading frequency was increased to 4 Hz. Subsequently, the ballast under the ties was rearranged, and the entire track was re-leveled. A long I-Beam Level was used to check the track in several locations including shoulders, cribs, over the ties, and over the rails. Afterwards, another round of seating load, which was equivalent to the first round, was applied. Although a slight differential displacement was observed at the start of the test, the track response rapidly stabilized, indicating that the track section had reached a more stable and leveled initial condition.

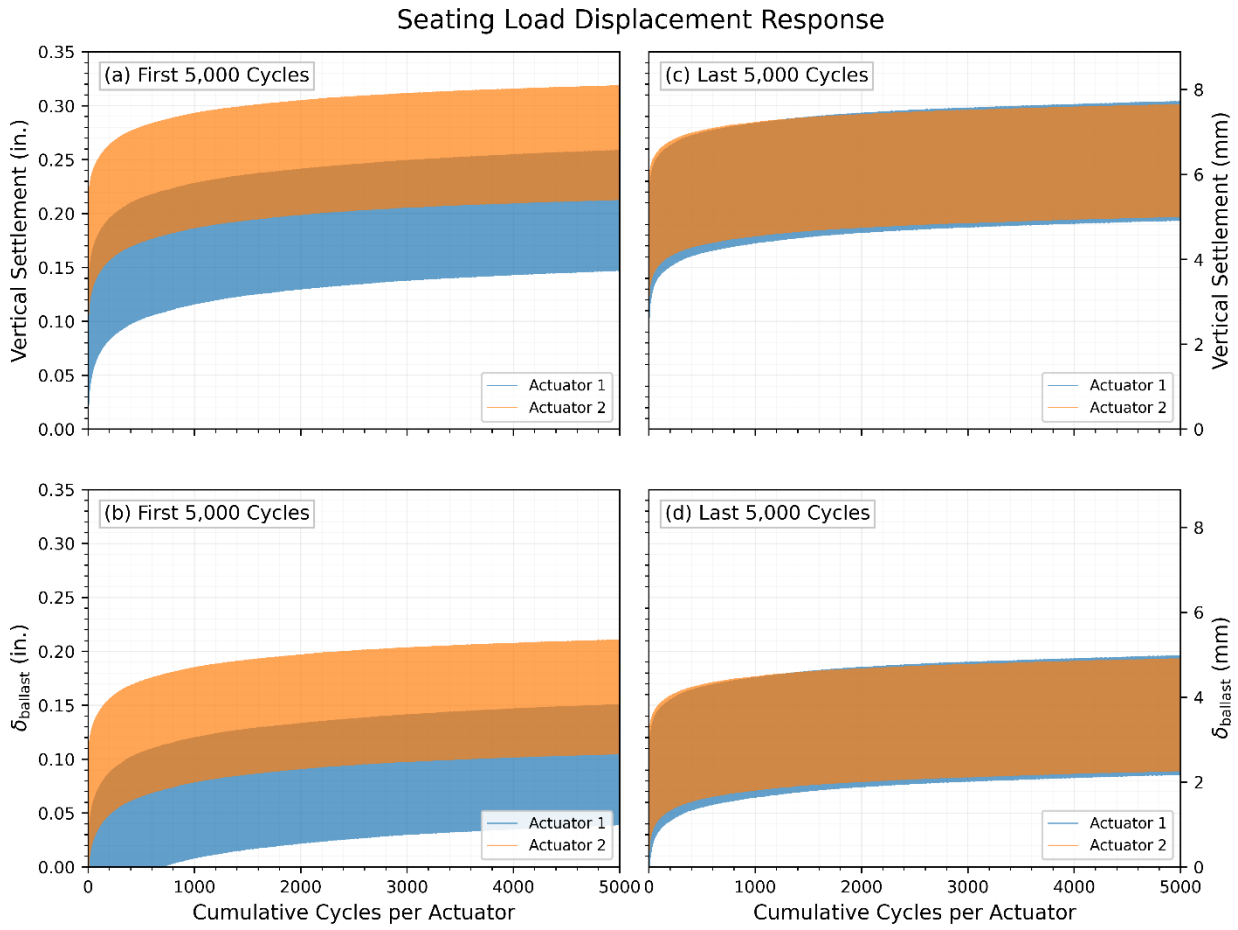


Figure 14: Seating load sequence applied to the track

The load-displacement data recorded by the MTS actuators was also used to evaluate the stiffness of the track section. In ballast box testing, the rigid boundaries of the box restrict lateral and longitudinal ballast movement, while the underlying concrete floor provides a rigid foundation. Under repeated loading, vertical displacement is therefore influenced primarily by the rearrangement, redistribution, and densification of the ballast and compacted limestone sand supporting the ties. As the granular materials become progressively seated, the incremental settlement generally decreases, resulting in an increase in the apparent stiffness of the track system. This response reflects the confined laboratory conditions, whereas field track behavior may additionally be influenced by subgrade deformation, ballast fouling, drainage conditions, and other environmental and operational factors.

The stiffness parameter calculated in this study is referred to as equivalent track stiffness, k_{eq} rather than track stiffness or track modulus. It represents the cyclic stiffness of the confined laboratory track system derived from the measured load-displacement response. For each loading cycle and based on each actuator, it was calculated as:

$$k_{(eq,i)} = \frac{\Delta P_i}{(\Delta \delta_i) \times s}$$

Where, $\Delta P_i = P_{(peak,i)} - P_{(valley,i)}$ is the measured load range for every cycle, $\Delta \delta_i = \delta_{(peak,i)} - \delta_{(valley,i)}$ is the corresponding cyclic displacement range, and s is the tie spacing. Figure 15 shows the load–displacement hysteresis response and equivalent track stiffness for the seating load. Because k_{eq} was calculated from the cyclic load and displacement ranges, differences in the absolute displacement response

between the two actuator locations did not directly affect the calculated stiffness. Similarly, the calculated stiffness is unchanged whether the actuator vertical settlement or the corrected ballast settlement is used, since the constant displacement correction does not affect $\Delta\delta$. As shown in Figure 15c, the equivalent stiffness increased gradually with continued seating cycles. Beyond approximately 6,000 cycles, k_{eq} remained about 4.9% higher than the value at the beginning of the test (average of the first 500 cycles), indicating a modest increase in stiffness as track became increasingly seated. Although Actuator 2 exhibited slightly higher equivalent stiffness than Actuator 1, the two responses remained closely comparable. The average cyclic load ranges were approximately 20.2 (90) and 20.1 kip (89 kN) for Actuators 1 and 2, respectively, while the corresponding displacement ranges were approximately 0.11 (2.794) and 0.10 in (2.54 mm). The slightly smaller cyclic displacement range measured at Actuator 2 therefore resulted in its slightly higher k_{eq}.

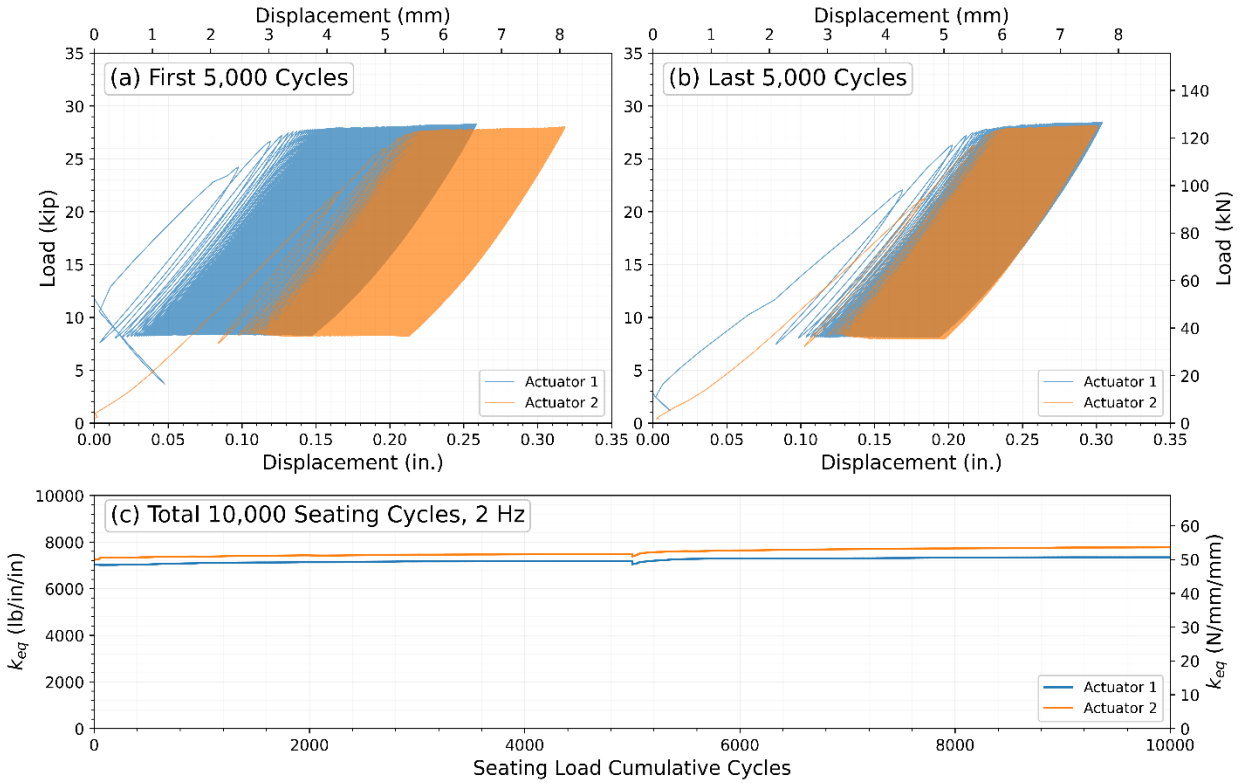


Figure 15: Load-displacement behavior and equivalent stiffness of the track

After application of the seating load, the nominal load magnitude was increased to 65 kip (289 kN) (refer to Table 4 for the achieved load), and the track was subjected to a total of 364,615 load cycles per actuator at a loading frequency of 2 Hz. Forensic reconstruction of the strain gauge response, presented later in this section, indicates that Tie 1 most likely cracked during the early stage of the first 65-kip loading set. This tie contained a localized fabrication defect, and although the fracture was not visually identified until later in the test, the evolution of the measured strain response indicates that substantial crack propagation or loss of local structural continuity occurred during this loading session. Following this event, Actuator 1 recorded substantially greater vertical displacement, resulting in a differential response between the two actuators again that persisted throughout the remainder of the test. To avoid disturbing the established ballast condition, the ballast was intentionally not rearranged or re-leveled thereafter. Consequently, results from both actuators are presented separately.

A sample of the first and final fatigue-loading sets is shown in Figure 16. As observed, ballast settlement beneath Actuator 1 continued to increase throughout the test until failure of the load spreader beam slightly before 380,000 cycles, at which point Actuator 1 reached the 6-in cylinder displacement limit (not shown

in the figure). In contrast, the response beneath Actuator 2 remained comparatively stable for most of the test, with a noticeable change occurring only near the end as the failure beneath Actuator 1 affected the overall loading system.

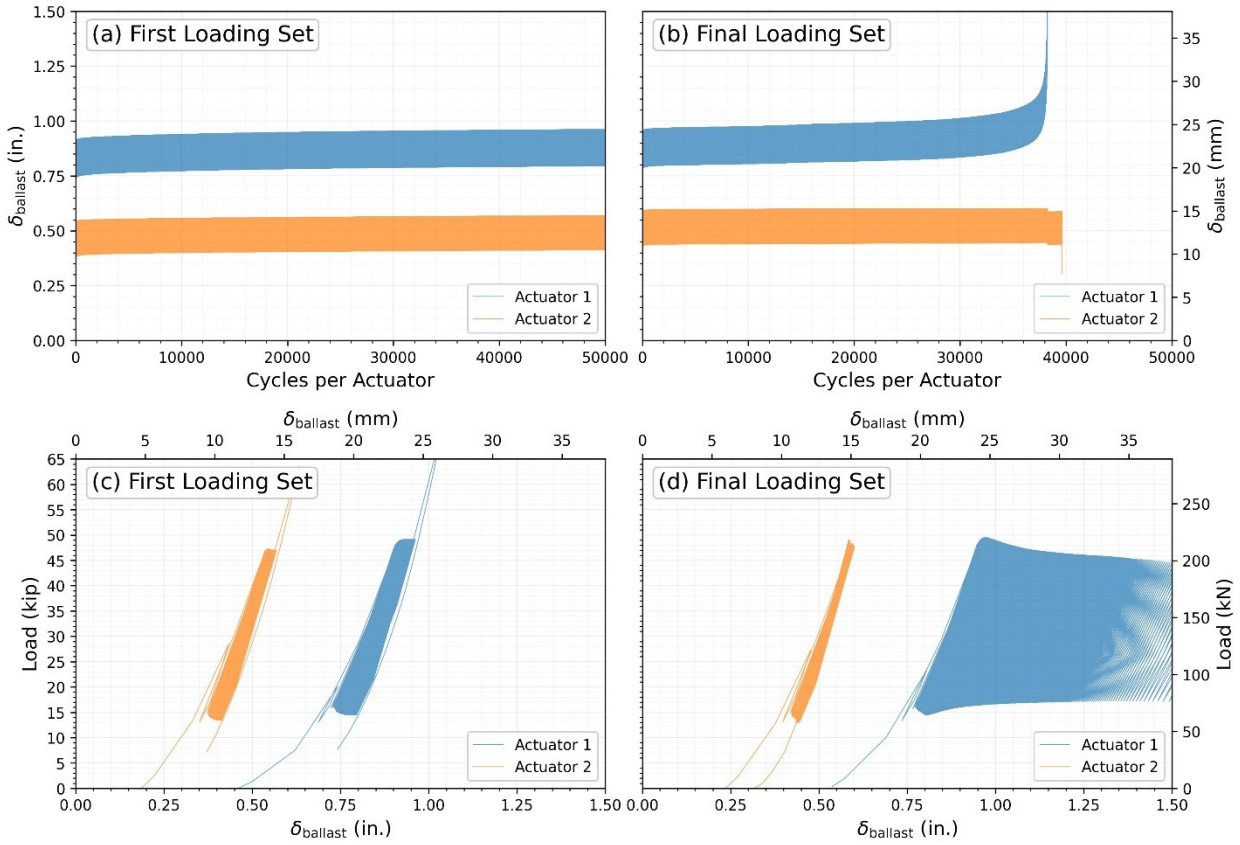


Figure 16: Load-displacement behavior for the track

Equivalent track stiffness during the test is shown in Figure 17. Throughout most of the test, the two actuator locations exhibited relatively stable stiffness responses, with Actuator 2 consistently showing slightly higher k_{eq} than Actuator 1. This difference is primarily associated with larger displacement range measured at Actuator 1, potentially due to cracking of Tie 1. Equivalent stiffness for Actuator 1 increased from approximately 7,956 to 8,420 lb/in/in by the end of the September 4 loading session, corresponding to an increase of approximately 5.8%. Based on Actuator 2, this is 4.8% (change from 8,356 to 8,757 lb/in/in).

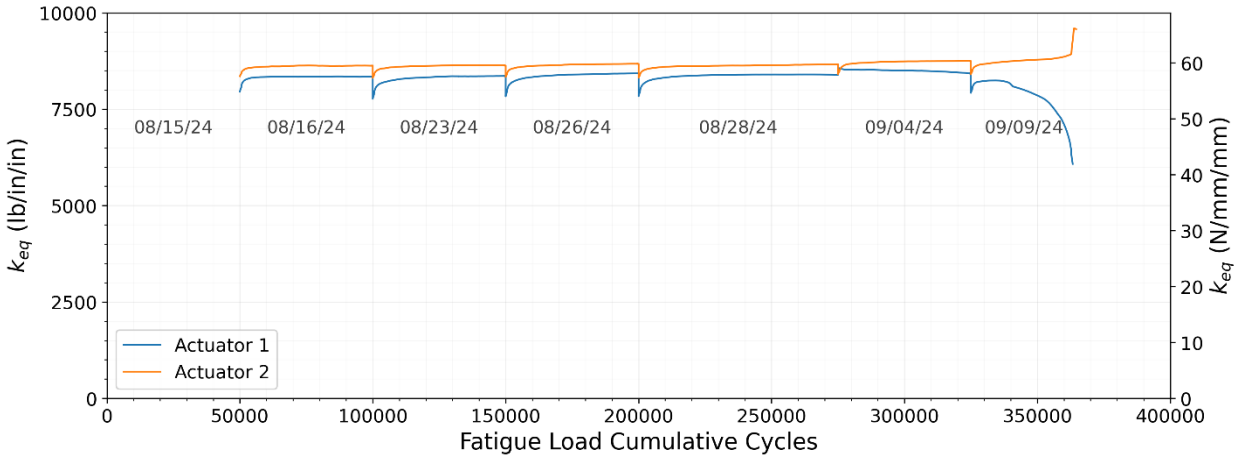


Figure 17: Equivalent track stiffness during the first available and last set of MTS loading data

3.3.2 Analytical Evaluation of Flexural and Shear Response

Figure 18 presents the analytical flexural and shear response of the EPC tie under the three loading configurations described in Section 2.4.2. Although the total applied load and assumed ballast reaction remained identical across the three models, the distribution of the rail seat loads influenced the resulting shear force, bending moment, stress, and strain distributions. The concentrated-load model represents an idealized loading condition, while the rail base and tie plate models account for the distribution of the applied load over progressively larger contact widths.

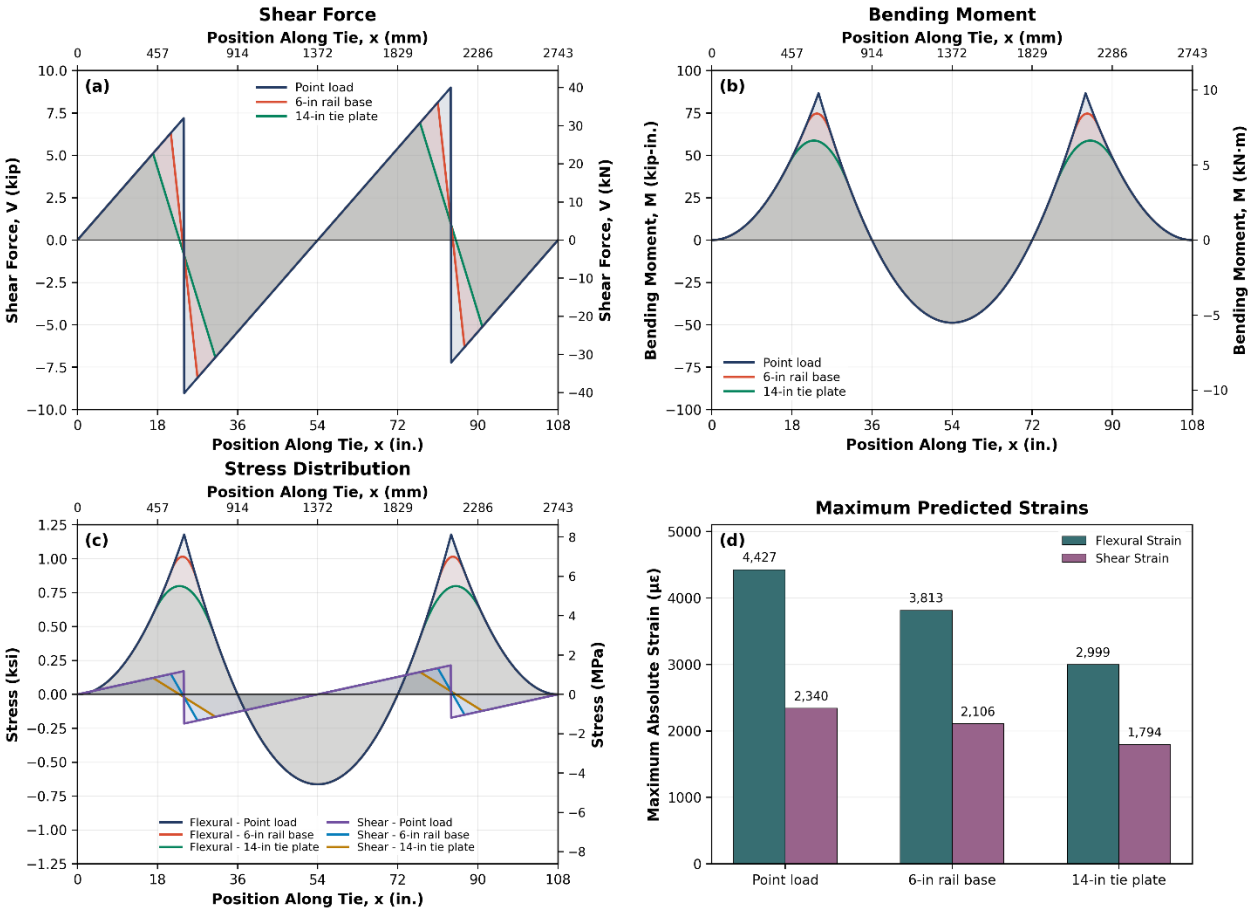


Figure 18. Analytical response of EPC ties under three rail seat loading configurations: (a) shear force distribution, (b) bending moment distribution, (c) flexural and shear stress distributions, and (d) comparison of maximum flexural and shear strains.

As shown in Figure 18(a), the maximum absolute shear force decreased from 9.03 kip (40.2 kN) for the concentrated-load model to 8.13 kip (36.1 kN) and 6.92 kip (30.8 kN) for the rail base and tie plate models, respectively. Similar effects were observed in the bending moment distributions (Figure 18(b)), where the maximum absolute bending moment decreased from 86.67 kip-in. (9.79 kN·m) to 74.65 kip-in. (8.43 kN·m) and 58.70 kip-in. (6.63 kN·m), respectively. The reductions were primarily associated with the redistribution of the applied loads near the rail seats.

The corresponding flexural and shear stress distributions are presented in Figure 18(c). The maximum absolute flexural stress decreased from 1.18 ksi (8.13 MPa) for the concentrated-load model to 1.02 ksi (7.00 MPa) and 0.80 ksi (5.51 MPa) for the rail base and tie plate models, respectively. Similarly, the

maximum absolute shear stress decreased from 0.215 ksi (1.48 MPa) to 0.193 ksi (1.33 MPa) and 0.165 ksi (1.14 MPa), respectively. Under all three loading configurations, the maximum shear stress was substantially lower than the maximum flexural stress, representing approximately 18–21% of the corresponding flexural stress magnitude. These results indicate that the flexural response is dominant under the assumed loading and support conditions, consistent with classical beam mechanics.

The corresponding maximum absolute flexural and shear strains are compared in Figure 18(d). The calculated flexural strains were 4,427, 3,813, and 2,999 με for the concentrated-load, rail base, and tie plate models, respectively, while the corresponding shear strains were 2,340, 2,106, and 1,794 με. Although the calculated shear stresses were considerably smaller than the flexural stresses, the differences between their corresponding strains were less pronounced due to the lower shear modulus relative to the modulus of elasticity. Nevertheless, the maximum calculated shear strains remained approximately 53–60% of the corresponding maximum flexural strains across the three loading configurations.

Interestingly, the calculated strain magnitudes were generally comparable in order of magnitude to those obtained experimentally during the full-scale fatigue testing. The distributed fiber-optic measurements recorded longitudinal strains reaching approximately 4,311 με toward the end of testing, while the flexural strain gauges recorded absolute values of 3492 με. Likewise, the shear strain gauges registered strains between 3,000 to 4000 με, exceeding the maximum shear strain predicted by the simplified analytical models and, notably, the strains recorded by several flexural gauges. However, direct comparisons should be made cautiously. The analytical evaluation assumed homogeneous, isotropic, and linearly elastic material behavior, which may not fully represent the mechanical response of the extruded EPC material. Furthermore, the analytical values represent maximum sectional strains, whereas the strain gauges were positioned at specific locations that did not necessarily coincide with the theoretical maxima. The assumed uniform ballast reaction and idealized rail seat loading conditions may also differ from the actual load transfer mechanism developed during fatigue testing. Nevertheless, the analytical evaluation provides a useful reference for assessing the experimental strain magnitudes and highlights the relatively substantial shear strain response observed in the EPC ties, as discussed in the following subsections.

3.3.3 Flexural Strain Response

The overall flexural strain response of the four EPC ties is presented in Figure 19, including the seating load response and data from the subsequently cracked Tie 1 (refer to Figure 4 for the instrumentation layout). The recorded voltage for each strain gauge was converted to strain using manufacturer-supplied quarter bridge relationship as follows.

$$\varepsilon_{\mu\varepsilon} = -\frac{4V_{\text{out}}}{GF(V_{\text{ex}} + 2V_{\text{out}})} \times 10^6$$

Where GF = 2.0 is the strain gauge factor, V_{ex} = 2.5v is the excitation voltage, V_{out} is the recorded bridge output voltage. No baseline correction was applied to the e strain data in this study. The resulting strain was expressed in microstrain ($\mu\varepsilon$). The curves are color coded by test date, with the dates shown in the first subplot and applicable to all panels. Except for the anomalous response of Tie 1, particularly T1h2, the measured flexural strains generally remained within the $\pm 4000\ \mu\varepsilon$ range shown in the figure. The rail seat gauges (h1 and h3), and midspan gauge (h2) also show the strain states associated with rail seat in compression and midspan tension (tie center bending upward). Each subplot represents the strain history at a single fixed location on top of the side surface of the tie. The two interior ties (T2 and T3) exhibited similar overall response patterns, while T4 provides the corresponding response for the exterior tie position.

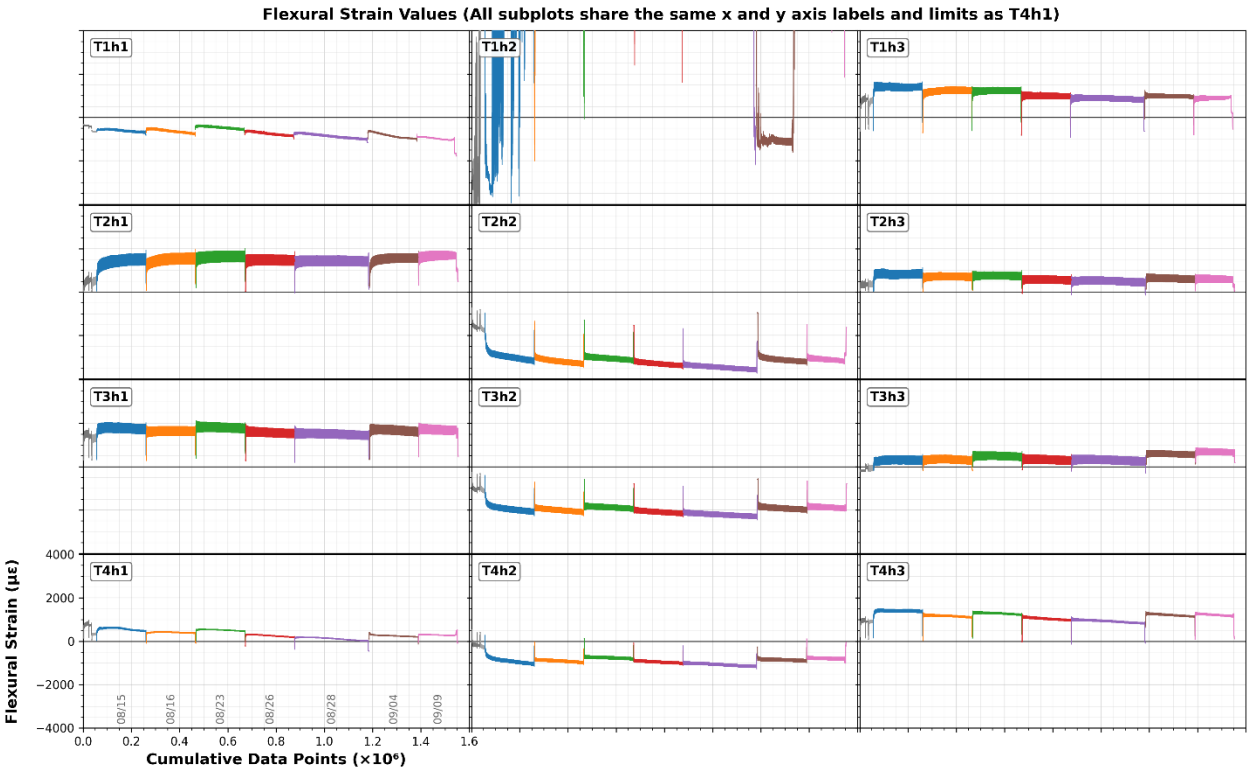


Figure 19: Flexural strain response measured by all strain gauges on the four EPC ties during the full-scale fatigue test.

In addition to the flexural strain histories presented in Figure 19, the daily mean strain values are calculated as well. For this analysis, Ties 2 and 3 were selected because both occupied interior positions within the track assembly, providing more comparable loading and support conditions than the exterior ties. Tie 1 was also affected by localized damage, as discussed later. The strain values were calculated directly from the recorded bridge output without baseline correction, consistent with Figure 19. Approximately 5% of the recorded data (2.5% from the beginning and 2.5% from the end of each testing session) were excluded when calculating the daily mean strain to minimize the influence of transient responses associated with initial actuator loading and final unloading. The standard deviation was calculated from the mean strain values of successive intervals within the retained data to characterize the variability during each testing session. Figure 20 presents the daily mean flexural strain values for Ties 2 and 3 at the two rail seat locations (h1 and h3) and midspan (h2).

As shown in Figure 20, both ties consistently exhibited positive mean strain values at the rail seat locations and negative values at midspan, corresponding to the general bending response observed in analytical method. However, the strain magnitudes differed between the two ties and varied across testing dates. Tie 3 generally exhibited higher positive strains at h1, whereas Tie 2 experienced substantially greater negative strains at h2. Despite these differences in magnitude, both ties exhibited similar changes in their recorded strain levels between several testing sessions. For instance, the flexural strain decreased on August 28 and was followed by a shift toward more positive recorded strain levels on September 4 and 9. The error bars indicate relatively limited within-session variation compared with the differences in mean strain levels observed between several testing dates.

These variations suggest that the recorded strain response was influenced by conditions extending beyond the immediate cyclic loading within individual testing sessions. Potential contributing factors include time-dependent material response, changes in ballast support and load distribution, and temperature-related effects on the tie material or strain measurement system which is discussed later.

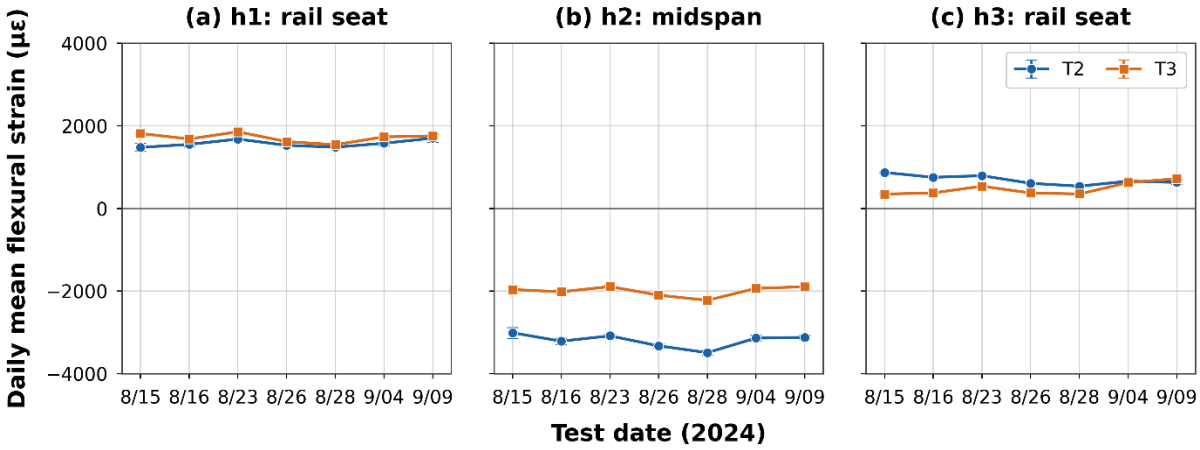


Figure 20. Daily mean flexural strain values for Ties 2 and 3 at (a) rail seat location h1, (b) midspan h2, and (c) rail seat location h3.

In addition to the strain histories and daily mean strain values, the cyclic strain amplitude was evaluated to characterize the magnitude of strain variation during repeated loading. Strain amplitude was calculated as half of the peak-to-peak strain range over successive 1,000-cycle intervals. Consistent with the daily mean strain analysis, approximately 5% of the recorded data (2.5% at each end of the testing session) were excluded to minimize the influence of initial loading and final unloading transients. Figure 21 presents the resulting daily mean cyclic strain amplitudes for Ties 2 and 3, with error bars representing the standard deviation of the strain amplitude during the day. Tie 2 generally exhibited higher strain amplitudes than Tie 3 at h1, whereas the amplitudes at h2 were relatively comparable. At h3, Tie 3 generally exhibited higher amplitudes until a noticeable reduction on September 4 and 9. Importantly, strain amplitude describes the magnitude of cyclic strain excursions and hence, these results should be interpreted together with Figures 19 and 20 rather than as a standalone measure of accumulated deformation or fatigue damage.

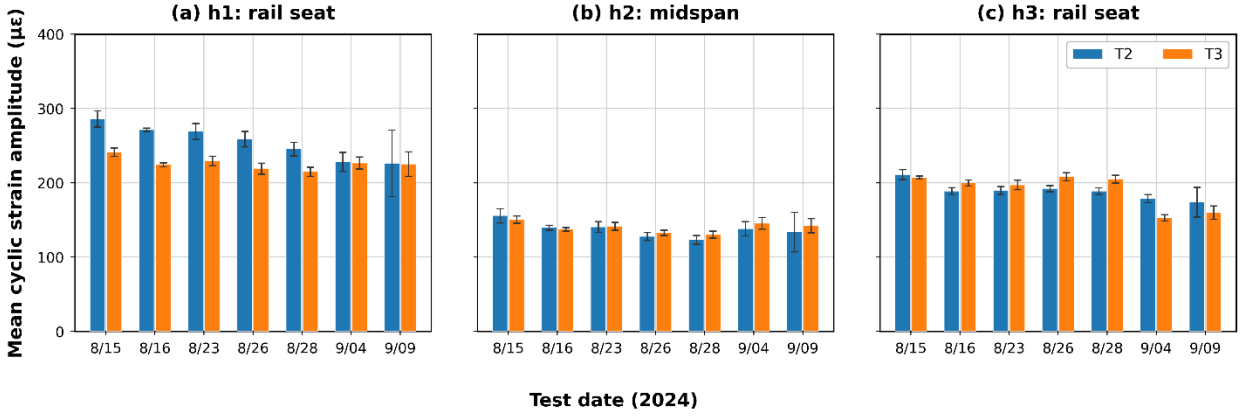


Figure 21. Daily mean cyclic flexural strain amplitudes for Ties 2 and 3 at (a) rail seat location h1, (b) midspan h2, and (c) rail seat location h3.

Across Ties 2-3, the cyclic strain amplitudes fluctuated within relatively consistent ranges throughout the fatigue test and did not exhibit a systematic progressive increase with increasing load cycles. Variations were observed between test sessions and among gauge locations, with the rail seat and midspan gauges reflecting the different strain amplitude trends.

3.3.4 Shear Strain Response

Shear strain was monitored on Tie 3 using three shear strain gauges positioned at the neutral axis beneath the rail seat region, as shown in Figure 4. Reported shear strains were converted to microstrain using their absolute values as $\gamma_{\mu\varepsilon} = |\gamma_{\text{recorded}}| \times 10^6$, where γ_{recorded} is the recorded dimensionless shear strain and $\gamma_{\mu\varepsilon}$ is the magnitude expressed microstrain. The resulting shear strain response throughout the fatigue test is presented in Figure 22. This figure also includes an embedded bar plot of daily mean outdoor air temperature during the test days for visual comparison. Flexural strain plots follow the same trend (Figure 19 and 20). A temperature correlation is presented in the next section. Unlike flexural strain, which primarily characterizes the longitudinal bending response, these measurements were intended to evaluate local shear deformation near the rail seat, where relatively high shear forces are expected. This is particularly important for composite ties because mechanisms such as matrix cracking, interfacial debonding, longitudinal splitting, and separation within the material can compromise its shear resistance. Once initiated, such damage may reduce the effective shear-resisting section and produce localized stress concentrations under repeated loading.

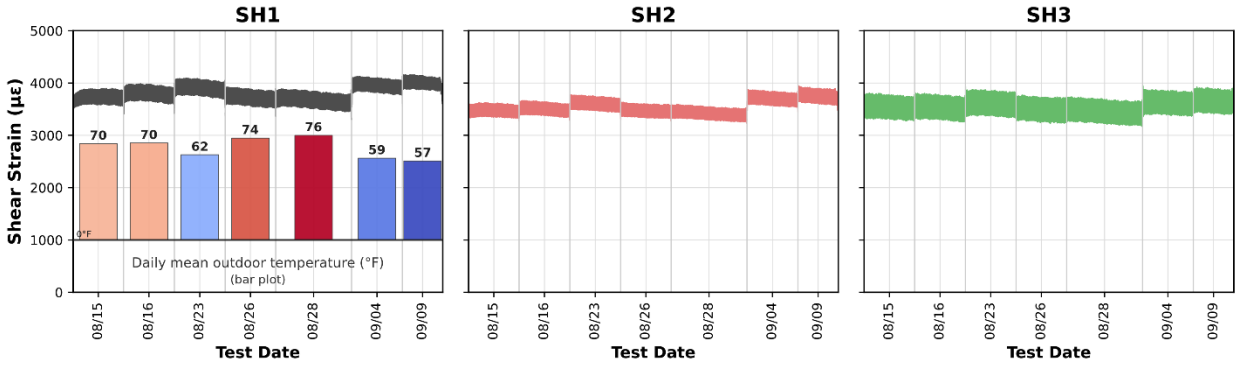


Figure 22: Shear strain response under one of the rail seat locations on Tie 3

As shown in Figure 22, all three gauges recorded relatively high shear strains throughout the fatigue test, generally ranging between approximately 3100 and 4100 με, SH1 or gauge side, exhibiting the highest values. Although some fluctuations and stepwise changes were observed between testing stages, the measured strains remained relatively stable and do not indicate continuous accumulation of shear strain. The magnitude of these measurements is particularly noteworthy when compared with the flexural strain response. While the flexural strain gauges recorded values below 2,000 με in most cases with maximum absolute value of about 3500 με, the shear strain gauges mostly recorded above 3,500 με. These measurements also exceeded the maximum shear strains of approximately 1,794–2,340 με estimated from the simplified analytical models in Section 3.3.2. Although the analytical models predicted substantially lower maximum shear stresses than maximum flexural stresses, the corresponding strain magnitudes depend on the material's shear modulus and modulus of elasticity, respectively. Furthermore, the analytical evaluation assumed homogeneous, isotropic, and linearly elastic behavior, whereas the actual EPC material consists of multiple polymer phases and mineral fillers, with potentially nonuniform mechanical properties and local interfacial characteristics. Such material heterogeneity, together with possible localized deformation near the rail seats, may contribute to the relatively high measured shear strains. Differences in sensor locations, actual ballast support conditions, tie plate eccentricity and rail seat cant must also be considered when comparing the measured and analytical responses. Therefore, while these measurements do not independently establish shear-related damage, their relatively high magnitudes highlight the significance of shear deformation in EPC railroad ties and emphasize the importance of evaluating shear behavior alongside flexural performance.

3.3.5 Temperature Correlation with Recorded Strain

Figure 23 presents the correlation between daily mean outdoor air temperature and daily mean recorded strain values obtained from the flexural and shear strain gauges. Among the three measurements, the shear strain exhibited the strongest negative correlation with temperature, with a Pearson correlation coefficient of −0.989 and an R^2 of 0.979, followed by the rail seat flexural strain ($r = -0.901$, $R^2 = 0.812$) and midspan flexural strain ($r = -0.769$, $R^2 = 0.592$). These results indicate that both flexural and shear strain measurements were associated with variations in outdoor air temperature, although the relationships differed between gauge locations. As temperature decreased, the recorded positive flexural strain at the rail seats and the shear strain magnitude increased, whereas the negative flexural strain at midspan became less negative, indicating a reduction in its absolute magnitude.

These responses are particularly relevant to the two critical locations of the EPC tie. At the rail seats, where both flexural and shear stresses are important, the simultaneous increase in recorded flexural and shear strain with decreasing temperature suggests a potential increase in combined recorded strain response under cooler conditions. Conversely, midspan exhibited the opposite trend in strain magnitude, indicating that the two locations may respond differently to air temperature variations under the same loading conditions. Although the study indicates strong correlations between outdoor air temperature and recorded strains, potential contributions from the temperature sensitivity of the strain gauges should also be considered, as their influence cannot be independently determined from the available data.

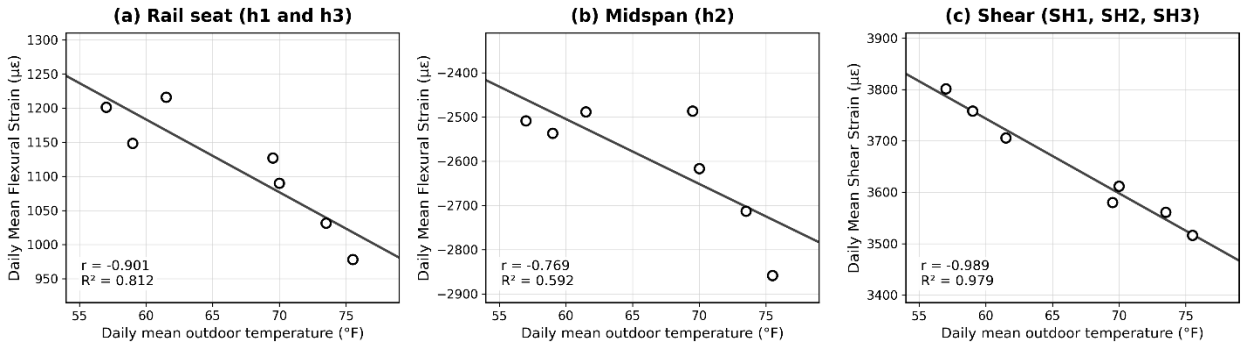


Figure 23. Correlation between daily mean outdoor air temperature and (a) mean rail seat flexural strain (h1 and h3), (b) mean midspan flexural strain (h2), and (c) mean shear strain (SH1, SH2, and SH3).

3.3.6 Distributed Fiber Optic Strain Response

The longitudinal strain response of Tie 3 was further evaluated using distributed fiber optic sensors installed along the upper and lower side surface of the tie, as described in Section 2.4.1 and shown in Figure 4. Unlike conventional strain gauges, which provide measurements at discrete locations, the fiber optic allows for continuous strain measurements. Figure 24 presents the strain distributions recorded during selected stages of fatigue testing, along with the corresponding envelopes.

As observed, during the seating stage on August 13 and 14, under a nominal actuator load of 35 kip, the maximum tensile strains along the upper run were approximately 2,318 and 2,109 με, respectively. Following the increase to the nominal 65-kip loading, the maximum strain reached 4,311 με and remained around 4,000-4,300 με during subsequent measurements.

The upper and lower sensor runs exhibited different strain magnitudes which may indicate an apparent shift in the neutral axis from the geometric center of the section, although differences in sensor positions and nonuniform material properties may also contribute. Despite fluctuations in the measured strains between testing dates, the general shapes and locations of the major strain peaks remained relatively consistent. In particular, the maximum upper run strains fluctuated around 4,000-4,300 με rather than increasing

progressively, suggesting no clear indication of continuous fatigue related strain accumulation during the recorded period.

Pronounced strain concentrations were observed near the rail seat regions and the tie midpoint. Notably, the highest tensile strains along the upper run were concentrated toward the side of the track where Tie 1 experienced an early fracture, possibly during the seating stage. The associated changes in track support and load distribution may have contributed to the asymmetric strain response.

Another notable observation was the substantial negative strain recorded along the upper run near the tie midpoint, accompanied by positive strain along the lower run. This potentially indicates center binding, a recognized concern in railroad ties, when support becomes concentrated near the tie center, resulting in increased central bending demands.

Likewise, the distributed measurements demonstrate that the flexural strain response can vary substantially along the tie and that localized strain magnitudes may exceed those captured by discrete strain gauges. This highlights the advantage of distributed fiber optic sensing in characterizing the spatial variability of deformation in EPC railroad ties.

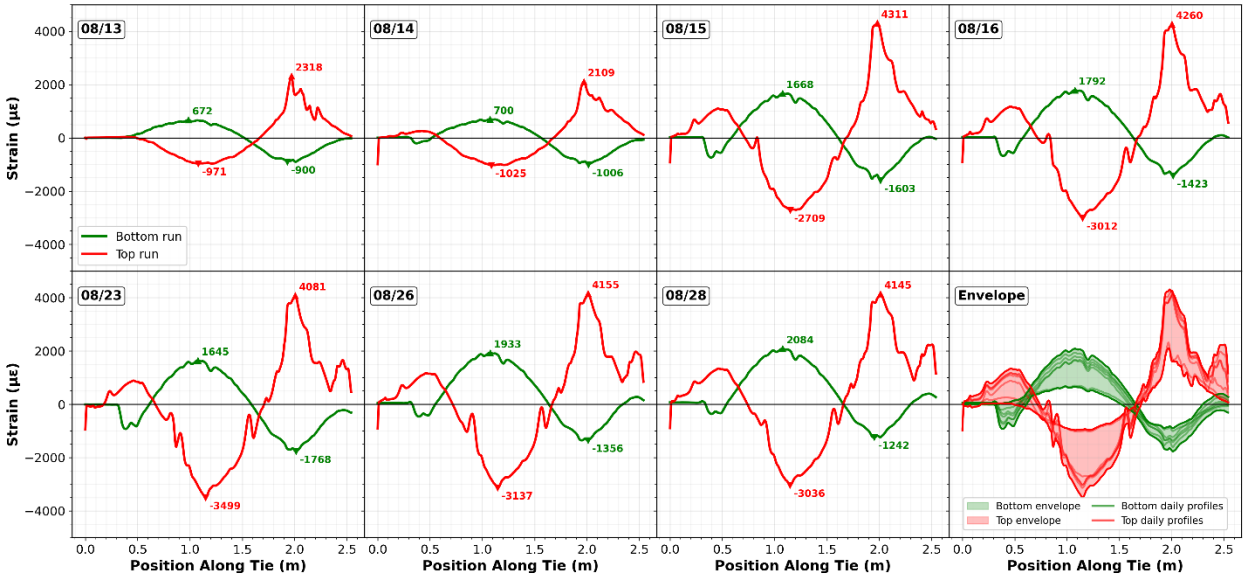


Figure 24: Flexural strain response of Tie 3 using fiber optic sensor data

3.4 Post-fatigue Forensic Analysis

Following completion of the full-scale fatigue testing, a post-fatigue investigation was conducted to evaluate the residual mechanical capacity of the EPC ties and examine physical evidence of damage and failure. The assessment consisted of destructive mechanical testing of the fatigued ties and forensic examination of the tie that cracked during fatigue testing.

3.4.1 Residual Mechanical Performance

The EPC ties that remained intact following the full-scale fatigue test were subsequently evaluated using the same three-point bending procedure described in Section 2.2. Figure 25 compares the stress-strain response, modulus of elasticity (MoE), and modulus of rupture (MoR) of the fatigued ties with those of ties tested in their original, unfatigued condition. Because the three-point bending test is destructive, the comparison represents two separate specimen groups, consisting of two unfatigued ties and three fatigued ties.

As shown in Figure 25, the fatigued ties exhibited reductions in both stiffness and flexural strength. The average MoE decreased from 266,353 ± 6,557 psi for the unfatigued ties to 249,444 ± 19,343 psi for the

fatigued ties, corresponding to a reduction of approximately 6.35%. In comparison, the average MoR decreased from 3,491 ± 946 psi to 2,334 ± 694 psi, representing a larger reduction of approximately 33.14%. The relatively modest reduction in MoE, together with the more pronounced reduction in MoR, suggests that the ultimate flexural capacity may have been more affected by repeated loading than the overall elastic stiffness. This trend is also evident in the stress-strain response, where the fatigued ties retained a broadly similar initial response but reached lower ultimate stress levels.

Greater variability was also observed in the MoE of the fatigued specimens. Considering the limited number of specimens, this difference should be interpreted cautiously; however, it may reflect nonuniform accumulation of fatigue damage among the ties. Within the ballast box configuration, the ties were not subjected to identical loading environments. Ties 2 and 3, located within the interior of the test section, experienced broadly similar loading conditions, whereas Ties 1 and 4 were subjected to somewhat different load-transfer conditions. Consequently, differences in accumulated damage prior to destructive testing may have contributed to the observed specimen to specimen variability in residual mechanical response.

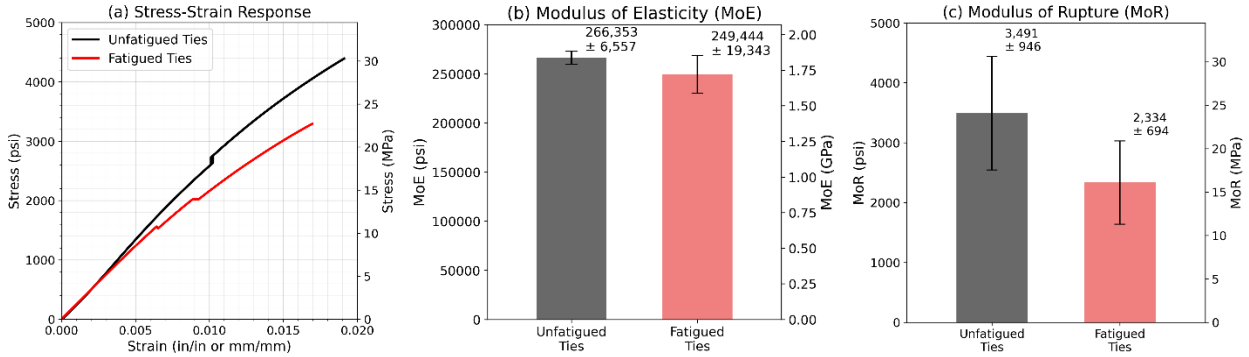


Figure 25: Mechanical performance of the fatigued and unfatigued ties

3.4.2 Forensic Analysis of the Fractured Tie

One of the four EPC ties (Tie 1) fractured during the fatigue test. Although the fracture was not visually identified until the later stages of testing, recorded strain history suggests that the tie may have experienced damage in the very early stage of the test. As shown in Figure 26, Tie 1 also carried a pronounced manufacturing defect along one face of the tie. Furthermore, examination of the fractured cross section further revealed internal irregularities and discontinuities, indicating that the affected region had compromised structural integrity. Hence, the pre-existing manufacturing defect may have contributed to the initiation and propagation of cracking under repeated loading. As shown in Figure 26, the strain response exhibited substantial fluctuations and increasingly irregular behavior during the seating stage under the nominal 35-kip load. Considering these observations together with the post-test forensic evidence, it is likely that cracking initiated during seating load and that the tie fractured during the first set of main fatigue loading. The early fracture of Tie 1 may also have influenced the subsequent behavior of the track assembly by altering the local stiffness, support conditions, and distribution of loads among the adjacent ties. This may have contributed to some of the nonuniform displacement and strain responses observed during the full-scale testing, and the significant differential downward displacement between the two actuators.

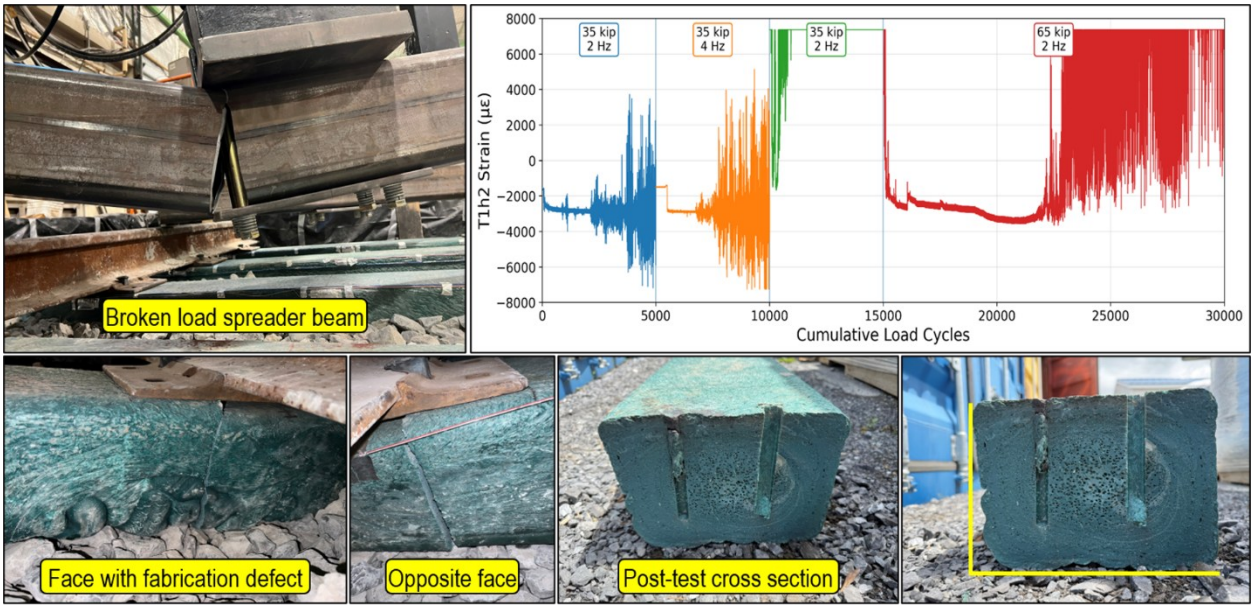


Figure 26: Forensic examination of fractured EPC Tie 1, showing the load spreader beam failure, recorded strain history for the first 30,000 cycles, visible manufacturing defects and cracking, and cross-sectional observations.

4.0 Conclusions and Recommendations

This study evaluated the fatigue performance of Engineered Polymer Composite (EPC) railroad ties through initial mechanical characterization, small-scale fatigue testing, full-scale ballast box testing, analytical evaluation, temperature correlation with recorded strains and post-fatigue mechanical and forensic investigations.

Initial mechanical characterization demonstrated favorable flexural and compressive properties, with an average modulus of elasticity (MOE) of 266,353 psi (1,836 MPa), modulus of rupture (MOR) of 3,491 psi (24.1 MPa), and rail seat compression deformation of 0.2331 in. (5.92 mm) under a 100-kip (445-kN) load. Small-scale fatigue testing showed relatively stable flexural stiffness, with apparent stiffness-based damage remaining below 1% over one million loading cycles at strain amplitudes of 800 and 1,000 με. An initial reduction in stiffness was followed by partial recovery and stabilization, with no evidence of sustained progressive stiffness degradation under the investigated conditions.

The full-scale ballast box experiment subjected four EPC ties to 379,615 loading cycles per actuator, including the initial seating stage. The track exhibited progressive settlement during seating, followed by comparatively stable cyclic behavior and modest increases in equivalent track stiffness. However, persistent differential displacement between the two actuator locations demonstrated the influence of nonuniform support conditions and load distribution. The early fracture of Tie 1, which contained a substantial manufacturing defect, likely contributed to this nonuniform response.

The analytical evaluation demonstrated that maximum shear stresses were considerably lower than maximum flexural stresses under the assumed loading conditions, while the corresponding shear strains represented approximately 53–60% of the calculated maximum flexural strains. Experimentally, the shear gauges registered relatively high strain magnitudes, generally ranging from approximately 3,100 to 4,100 με, while distributed fiber optic measurements identified localized longitudinal strains reaching approximately 4,311 με. These findings highlight the importance of evaluating localized flexural and shear responses in EPC railroad ties. The recorded strain histories also showed no consistent progressive accumulation of strain in the intact ties. Furthermore, strong correlations were observed between daily mean

outdoor air temperature and recorded flexural and shear strains, although potential temperature-related measurement effects could not be independently quantified.

Post-fatigue mechanical testing revealed average reductions of approximately 6.35% in MOE and 33.14% in MOR compared with the unfatigued specimens. The greater reduction in flexural strength suggests that ultimate load-carrying capacity may be more sensitive to repeated loading than elastic stiffness. However, the limited specimen population and differences in initial material properties prevent these reductions from being attributed exclusively to fatigue damage. Forensic examination of the fractured Tie 1 revealed internal discontinuities and impurities with substantial manufacturing defects, with the recorded strain history suggesting that damage may have initiated during seating load and progressed during the early stages of main fatigue loading.

Overall, the findings demonstrate the importance of evaluating EPC railroad ties under simulated track conditions in addition to conventional mechanical characterization and isolated specimen testing. Although the developed EPC formulation exhibited favorable initial mechanical properties and relatively stable cyclic stiffness, the observed manufacturing defects, material heterogeneity, early tie fracture, and reduction in residual flexural strength indicate that further improvements and validation are necessary before the formulation can be considered for practical railroad applications. Future studies should investigate controlled material formulations and manufacturing processes, larger specimen populations, extended fatigue loading, further characterization of shear properties, and the combined effects of temperature and cyclic loading on EPC tie performance.

5.0 RESEARCH FUNDING

No dedicated research grant was received for the work reported in this study. The materials, molds, manufacturing, and shipment of the EPC railroad ties were generously provided by Eco Plastic Products, a registered 501(c)(3) nonprofit organization based in Wilmington, Delaware, through a collaborative research effort with the author. The experimental work was conducted by the author at the Civil Infrastructure Testing and Evaluation Laboratory (CITEL) at Penn State University Park and the Rail Transportation Engineering (RTE) Laboratory at Penn State Altoona.

6.0 CRediT AUTHOR STATEMENT

Jubair Ahmad Musazay: Conceptualization, Methodology, Validation, Formal Analysis, Investigation, Data Curation, Writing-Original Draft, Writing-Review & Editing, Visualization, Supervision, Project Administration, Resources.

7.0 ACKNOWLEDGMENT

The author acknowledges and appreciates Dr. Shihui Shen for serving as his doctoral advisor during certain stages of this research. Special appreciation is extended to Dr. Dr. Yuliang Zhou for his continued assistance throughout the experimental work. The author also thanks Dr. Kun Zhang, Vince Ferraro, Dan Fura, Thomas Hatch, and Jonathan Hileman for their contributions and assistance at different stages of the project. The contributions of North Shore Railroad Company & Affiliates (NSHR) and Railroad Technology & Services are also gratefully acknowledged. Finally, the author expresses deep appreciation to Dr. Charles Falletta and Jim Kelley of Eco Plastic Products in Delaware for their continued support through material supply, equipment, manufacturing, shipping, and technical expertise, without which this research would not have been possible.

8.0 DECLARATION OF COMPETING INTEREST

The author declares no known competing financial interests or personal relationships that could have appeared to influence the work reported in this paper.

9.0 ARTIFICIAL INTELLIGENCE DISCLAIMER

During the preparation and revision of this manuscript, the author used OpenAI's ChatGPT as an assistance tool for language editing, manuscript organization, proofreading, literature searches, and data processing. The author reviewed the AI-assisted work and takes full responsibility for the scientific interpretations, conclusions, and overall content of the manuscript.

10.0 REFERENCES

1. Manalo, A., T. Aravinthan, W. Karunasena, and A. Ticoalu. A Review of Alternative Materials for Replacing Existing Timber Sleepers. *Composite Structures*, Vol. 92, No. 3, 2010, pp. 603–611. https://doi.org/10.1016/j.compstruct.2009.08.046.
2. Ferdous, W., and A. Manalo. Failures of Mainline Railway Sleepers and Suggested Remedies – Review of Current Practice. *Engineering Failure Analysis*, Vol. 44, 2014, pp. 17–35. https://doi.org/10.1016/j.engfailanal.2014.04.020.
3. Ferdous, W., A. Manalo, G. Van Erp, T. Aravinthan, S. Kaewunruen, and A. Remennikov. Composite Railway Sleepers – Recent Developments, Challenges and Future Prospects. *Composite Structures*, Vol. 134, 2015, pp. 158–168. https://doi.org/10.1016/j.compstruct.2015.08.058.
4. Lampo, R., T. Nosker, B. Gillespie, and R. Schriks. Performance and Safety Issues Regarding the Use of Plastic Composite Crossties.
5. Lotfy, I., M. Farhat, M. A. Issa, and M. Al-Obaidi. Flexural Behavior of High-Density Polyethylene Railroad Crossties. *Proceedings of the Institution of Mechanical Engineers, Part F: Journal of Rail and Rapid Transit*, Vol. 230, No. 3, 2016, pp. 813–824. https://doi.org/10.1177/0954409714565655.
6. Ju, S., J. Yoon, D. Sung, and S. Pyo. Mechanical Properties of Coal Ash Particle-Reinforced Recycled Plastic-Based Composites for Sustainable Railway Sleepers. *Polymers*, Vol. 12, No. 10, 2020, p. 2287. https://doi.org/10.3390/polym12102287.
7. Ferdous, W., A. Manalo, C. Salih, P. Yu, R. Abousnina, T. Heyer, and P. Schubel. Behaviour of Polymer Filled Composites for Novel Polymer Railway Sleepers. *Polymers*, Vol. 13, No. 8, 2021, p. 1324. https://doi.org/10.3390/polym13081324.
8. Yu, P., A. Manalo, W. Ferdous, C. Salih, R. Abousnina, T. Heyer, and P. Schubel. Failure Analysis and the Effect of Material Properties on the Screw Pull-out Behaviour of Polymer Composite Sleeper Materials. *Engineering Failure Analysis*, Vol. 128, 2021, p. 105577. https://doi.org/10.1016/j.engfailanal.2021.105577.
9. Jimenez, R. *Vertical Track Modulus in Plastic Composite Ties Test Zones at FAST*. Publication DOT/FRA/ORD-03/13. Transportation Technology Center, Inc., Pueblo, CO, 2003.
10. Reiff, R., and C. Trevizo. *Cracking and Impact Performance Characteristics of Plastic Composite Ties*. Publication DOT/FRA/ORD-12/03. Transportation Technology Center, Inc., Pueblo, CO, 2012.
11. McHenry, M., Y. Gao, and J. P. Baillargeon. Implementing Improved Composite Tie Design and Testing Guidelines in the AREMA Manual for Railway Engineering. Presented at the AREMA Annual Conference, 2018.
12. Gao, Y., and M. McHenry. *Improved Polymer Composite Tie Performance*. Publication DOT/FRA/ORD-24-16. FRA, Washington, D.C., 2024, p. 51.
13. Woody, S., and J. Baillargeon. *Evaluation of Engineered-Polymer Composite Tie Performance in Revenue Service*. Publication RR 22-20. FRA DOT, Washington, D.C., 2022.
14. Salih, C. *STATIC AND FATIGUE BEHAVIOUR OF COMPOSITE RAILWAY SLEEPERS*. PhD. Southern Queensland, Toowoomba, Queensland, Australia, 2022.

15. Salih, C., A. Manalo, W. Ferdous, R. Abousnina, P. Yu, T. Heyer, and P. Schubel. Novel Bending Test Method for Polymer Railway Sleeper Materials. *Polymers*, Vol. 13, No. 9, 2021, p. 1359. https://doi.org/10.3390/polym13091359.
16. Salih, C., A. Manalo, W. Ferdous, P. Yu, T. Heyer, and P. Schubel. Behaviour of Timber-Alternative Railway Sleeper Materials under Five-Point Bending. *Construction and Building Materials*, Vol. 316, 2022, p. 125882. https://doi.org/10.1016/j.conbuildmat.2021.125882.
17. American Railway Engineering and Maintenance-of-Way Association (AREMA) Manual for Railway Engineering. AREMA, , 2026.
18. Salih, C., A. Manalo, W. Ferdous, R. Abousnina, P. Yu, T. Heyer, and P. Schubel. Novel Bending Test Method for Polymer Railway Sleeper Materials. *Polymers*, Vol. 13, No. 9, 2021, p. 1359. https://doi.org/10.3390/polym13091359.
19. Lotfy, I., and M. A. Issa. Evaluation of the Longitudinal Restraint, Uplift Resistance, and Long-Term Performance of High-Density Polyethylene Crosstie Rail Support System Using Static and Cyclic Loading. *Proceedings of the Institution of Mechanical Engineers, Part F: Journal of Rail and Rapid Transit*, Vol. 231, No. 8, 2017, pp. 835–849. https://doi.org/10.1177/0954409716647094.
20. Amjadi, M., and A. Fatemi. Creep and Fatigue Behaviors of High-Density Polyethylene (HDPE): Effects of Temperature, Mean Stress, Frequency, and Processing Technique. *International Journal of Fatigue*, Vol. 141, 2020, p. 105871. https://doi.org/10.1016/j.ijfatigue.2020.105871.
21. Van Belkom, A., M. Pittrich, and V. Lojda. Intermittent Cyclic Load Testing of Polymer Railway Sleepers. *Proceedings of the Institution of Mechanical Engineers, Part F: Journal of Rail and Rapid Transit*, Vol. 236, No. 7, 2022, pp. 816–825. https://doi.org/10.1177/09544097211045460.